

Chapter 12

QFI System Architecture

From Subsystem Integration to Production Deployment
With the Feasibility-Capability-Novelty (FCN) Framework

This chapter addresses **system-level integration** across the complete QFI operator stack, establishing quantitative relationships between architecture choices and the model-mismatch penalty Γ_{mm} .

Key Outputs:

- Architecture quality factor: $Q_{arch} = f(\text{coherence, throughput, drift})$
- Comprehensive SWOT analysis for 0D/1D/2D/3D architectures
- FCN Framework for quantitative technology assessment
- Risk mitigation strategies and error budget allocation

Central Question: How do system architecture uncertainties propagate to reconstruction fidelity, and how can we optimize architecture selection using the FCN framework?

QFI Pipeline Position:

$$S(\mathbf{r}) \xrightarrow{\mathcal{G}} F(\mathbf{r}) \xrightarrow{\boxed{\mathcal{M}}} D(\mathbf{r}) \xrightarrow{\mathcal{R}} \hat{S}(\mathbf{r}) \pm \sigma_S$$

Table 12.1: Abbreviated terms used in Chapter 12.

Abbrev.	Full Term	Abbrev.	Full Term
AOM	Acousto-Optic Modulator	MW	Microwave
AWG	Arbitrary Waveform Generator	NA	Numerical Aperture
DAQ	Data Acquisition	NV	Nitrogen-Vacancy
EMI	Electromagnetic Interference	ODMR	Optically Detected Mag. Resonance
FCN	Feasibility-Capability-Novelty	PIC	Photonic Integrated Circuit
FOV	Field of View	PRNU	Photo-Response Non-Uniformity
FPGA	Field-Programmable Gate Array	QFI	Quantum Field Imaging
GPU	Graphics Processing Unit	QFM	Quantum Field Metrology
IC	Integrated Circuit	sCMOS	Scientific CMOS
MEMS	Micro-Electro-Mechanical Sys.	SiN	Silicon Nitride

Abstract

This chapter presents a comprehensive treatment of Quantum Field Imaging (QFI) system architecture, addressing the critical challenge of integrating optical subsystems with forward models while maintaining quantum state coherence and measurement fidelity. We develop architecture theory from first principles, establishing quantitative relationships between system parameters and the model-mismatch penalty Γ_{mm} .

The chapter introduces a novel architectural taxonomy spanning 0D (point-like), 1D (waveguide), 2D (planar), and 3D (volumetric) implementations, with detailed SWOT analysis and risk mitigation strategies for each approach. We demonstrate that system architecture uncertainties directly impact quantum state control, with decoherence-architecture coupling factors quantified through rigorous error propagation analysis.

A key contribution is the **Feasibility-Capability-Novelty (FCN) Framework**, a quantitative methodology for evaluating emerging photonic architectures that goes beyond traditional SWOT analysis. The FCN framework enables investment prioritization, bottleneck identification, and technology roadmap planning through composite scoring across three orthogonal dimensions.

The end-to-end *QIFOM* budget framework enables practitioners to optimize resource allocation across subsystems for maximum imaging fidelity. Six worked examples demonstrate FCN analysis, error budget allocation, and architecture selection for production QFI systems.

12.1 Introduction: Why System Architecture Matters

12.1.1 The Integration Challenge

The previous chapters have developed the theoretical foundations of Quantum Field Imaging through the operator stack framework: $S \rightarrow G \rightarrow F(r) \rightarrow M \rightarrow D \rightarrow R \rightarrow \hat{S}$. Each operator has been optimized in isolation, but production QFI systems require seamless integration where:

1. **Subsystem interfaces** must preserve signal fidelity
2. **Calibration protocols** must account for cross-subsystem dependencies
3. **Error budgets** must be allocated to maximize end-to-end performance
4. **Architecture choices** must balance competing requirements



Figure 12.1: QFI system architecture overview. (a) Complete operator stack with subsystem mapping. (b) Photon budget cascade from excitation to detection. (c) Error propagation pathways. (d) Architecture decision tree.

12.1.2 Historical Context

System architecture for quantum sensing has evolved through three generations:

Table 12.2: Evolution of quantum sensing system architecture.

Generation	Era	Characteristic	Limitation
1st	2008–2015	Lab benchtop, manual alignment	Single-point, hours/measurement
2nd	2015–2022	Integrated modules, automated	Wide-field but not production
3rd	2022–present	Production-grade, dockable	Emerging; this chapter’s focus

12.1.3 Pain Points in Current Approaches

Table 12.3: System architecture pain points and their impacts.

Pain Point	Root Cause	Impact on Γ_{mm}
Thermal drift	Inadequate athermal design	5–15% Γ_{mm} degradation
MW inhomogeneity	Antenna-objective interference	3–10% spatial Γ_{mm} variation
Optical misalignment	Vibration, creep	2–8% throughput loss
Calibration drift	Environment changes	Requires re-calibration every 4–8 hours
Subsystem crosstalk	EMI, optical leakage	False signals, reconstruction artifacts

12.1.4 Chapter Objectives

This chapter will:

1. Develop a comprehensive **system block diagram** with operator mapping
2. Present an **architectural taxonomy** (0D, 1D, 2D, 3D) with trade-offs
3. Provide **SWOT analysis** for each architecture class
4. Introduce the **FCN Framework** for quantitative technology assessment
5. Establish **error budget methodology** for Γ_{mm} optimization
6. Deliver **worked examples** for production system design

12.2 System Block Diagram and Operator Mapping

12.2.1 Complete System Architecture

Figure 12.2 presents the complete QFI system architecture with explicit mapping to the operator stack.

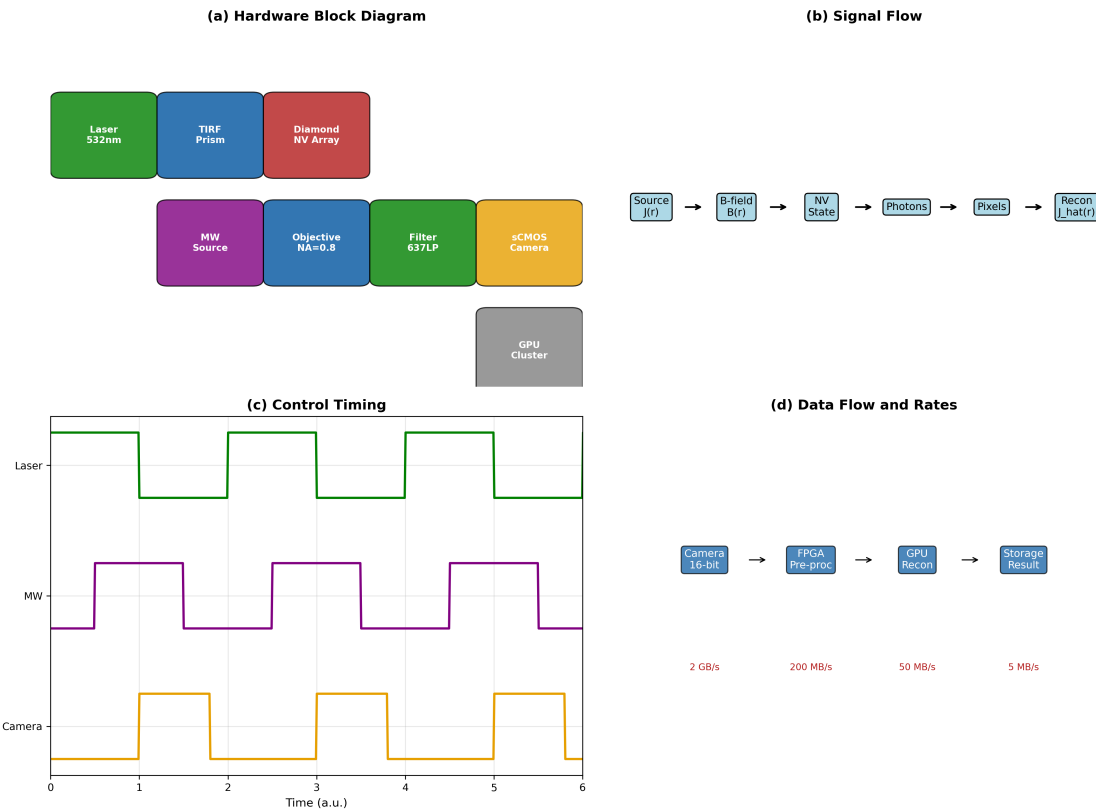


Figure 12.2: Complete QFI system block diagram. (a) Hardware subsystems with operator mapping. (b) Signal flow from source to reconstruction. (c) Control and synchronization pathways. (d) Data flow architecture.

12.2.2 Subsystem-to-Operator Mapping

Table 12.4: Subsystem-to-operator mapping in QFI systems.

Operator	Hardware Subsystem	Key Parameters	Chapter Ref.
S (Source)	Device under test	$J(\mathbf{r}), T(\mathbf{r})$	Ch. 10–11
\mathcal{G} (Forward)	Physics model	Biot-Savart, thermal	Ch. 10–11
\mathcal{F} (Collection)	Objective, tube lens	NA, η_{opt}	Ch. 4
\mathcal{M} (Measurement)	NV array, MW, camera	T_2 , contrast, QE	Ch. 7–9
D (Data)	DAQ, FPGA	Bit depth, frame rate	Ch. 9
\mathcal{R} (Reconstruction)	GPU cluster	Γ_{inv} , latency	Ch. 12

12.2.3 Photon Budget Cascade

The system-level photon budget follows a multiplicative cascade:

Key Equation: Photon Budget Cascade

$$N_{\text{detected}} = N_{\text{exc}} \cdot \eta_{\text{abs}} \cdot \text{QY} \cdot \eta_{\text{coll}} \cdot \eta_{\text{opt}} \cdot \eta_{\text{filter}} \cdot \text{QE} \quad (12.1)$$

Table 12.5: Photon budget cascade for typical QFI system.

Stage	Parameter	Typical Value	Cumulative
Excitation	N_{exc}	10^{12} photons/s	10^{12}
Absorption	η_{abs}	0.3	3×10^{11}
Quantum yield	QY	0.7	2.1×10^{11}
Collection (NA=0.8)	η_{coll}	0.2	4.2×10^{10}
Optics transmission	η_{opt}	0.7	2.9×10^{10}
Spectral filtering	η_{filter}	0.8	2.4×10^{10}
Detector QE	QE	0.85	2.0×10^{10}
End-to-end	η_{total}	0.02	—

12.3 Architectural Taxonomy: From 0D to 3D

We classify QFI architectures by their spatial dimensionality, which fundamentally determines parallelism N_{parallel} , achievable resolution δx , and the model-mismatch factor Γ_{mm} . This section develops each architecture from first principles, deriving performance metrics from physical parameters and establishing quantitative design trade-offs.

12.3.1 Architecture Classification Framework

Before examining each architecture in detail, we establish the classification criteria and key performance equations that will be applied consistently.

Definition 12.3.1 (Architecture Dimensionality). The **dimensionality** of a QFI architecture refers to the number of spatial dimensions over which NV centers are interrogated simultaneously in a single measurement cycle:

- **0D**: Single NV (or small cluster) at one point; image built by scanning
- **1D**: Linear array of NV centers; 2D image via 1D scanning
- **2D**: Planar NV array with wide-field readout; direct 2D imaging
- **3D**: Volumetric NV distribution; tomographic or light-sheet readout

The fundamental trade-off across architectures is captured by:

Key Equation: Architecture Trade-off Relation

$$Q_{\text{IFOM}} = \underbrace{\eta_q \cdot \sqrt{N_{\text{parallel}}}}_{\text{Sensitivity-Parallelism}} \cdot \underbrace{\Gamma_{\text{inv}} \cdot \Gamma_{\text{mm}}}_{\text{Reconstruction Fidelity}} \quad (12.2)$$

where higher dimensionality increases N_{parallel} but typically decreases Γ_{mm} due to calibration complexity.

12.3.2 2D Architecture: Planar Wide-Field Imaging

The 2D planar architecture is the primary candidate for production QFI systems, offering the optimal balance between parallelism and calibration fidelity for semiconductor failure analysis applications.

Definition 12.3.2 (2D Planar QFI Architecture). A **2D Planar QFI System** employs a thin layer of NV centers in a diamond membrane, interrogated by wide-field optical excitation and imaged onto a 2D detector array, enabling simultaneous measurement across 10^5 – 10^7 spatial channels.

12.3.2.1 System Schematic and Component Layout

Figure 12.3 presents the complete 2D QFI system architecture with all optical and electronic subsystems.

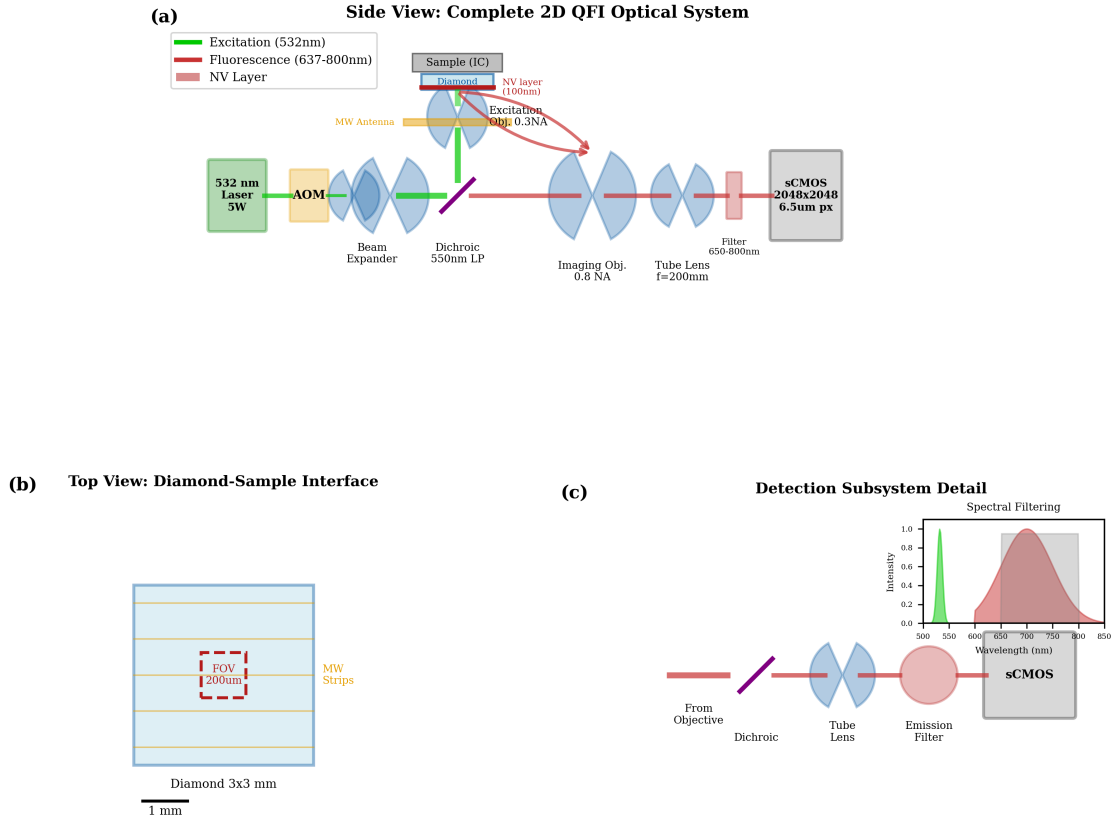


Figure 12.3: Complete 2D planar QFI system schematic. (a) Side view showing optical excitation path (green, 532 nm), fluorescence collection path (red, 637–800 nm), and MW delivery. (b) Top view of diamond-sample interface geometry. (c) Detection subsystem with spectral filtering. (d) Control and synchronization architecture.

System Components:

Table 12.6: 2D QFI system component specifications.

Subsystem	Component	Specification	Function
Excitation	Laser source	532 nm, 5 W CW	NV excitation
	AOM	80 MHz, >80% efficiency	Pulse modulation
	Beam expander	$10\times$, $M^2 < 1.2$	Uniform illumination
	Excitation objective	0.3 NA, 20 mm WD	Wide-field delivery
Collection	Imaging objective	0.8 NA, 3.5 mm WD	High-NA collection
	Tube lens	$f = 200$ mm	Image formation
	Dichroic mirror	550 nm long-pass	Excitation rejection
	Emission filter	650–800 nm bandpass	Spectral selection
Detection	sCMOS camera	2048×2048 , 6.5 μm	Image capture
	Quantum efficiency	95% at 700 nm	Photon conversion
	Frame rate	100 fps full frame	Temporal sampling
MW System	MW source	2.87 GHz, 10 W	NV spin manipulation
	Antenna	Microstrip, 50×50 mm 2	Field delivery
	AWG	1 GS/s, 14-bit	Pulse shaping
Sample Interface	Diamond membrane	50 μm thick, 3×3 mm 2	NV host
	NV layer	100 nm depth, 3 ppm	Sensing layer

12.3.2.2 Optical System Design

The optical system consists of two independent paths: excitation and collection.

Excitation Path Analysis The excitation path delivers uniform 532 nm illumination to the NV layer. The key design requirement is achieving <5% intensity variation across the field of view.

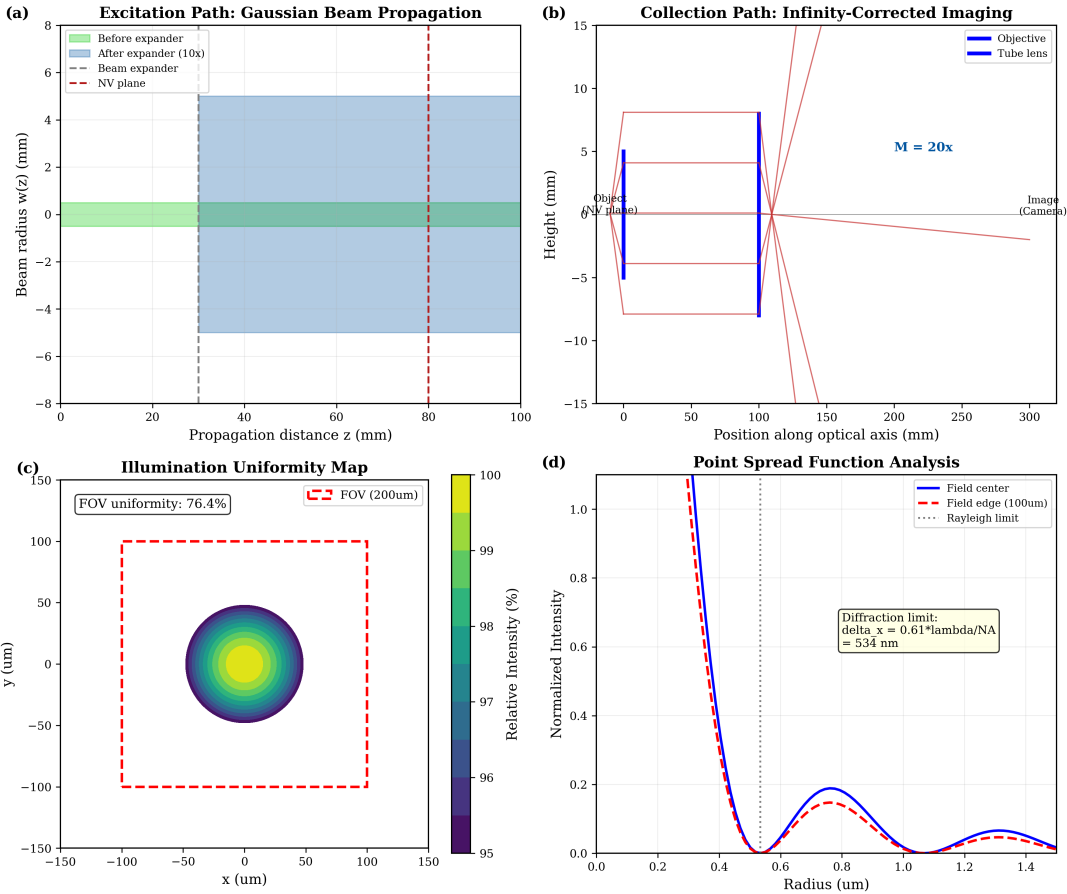


Figure 12.4: 2D system optical path analysis. (a) Excitation path ray trace with Gaussian beam propagation. (b) Collection path with infinity-corrected optics. (c) Illumination uniformity map. (d) PSF at field center and edge.

For a Gaussian beam with waist w_0 expanded to diameter D_{illum} :

$$I(r) = I_0 \exp\left(-\frac{2r^2}{w^2}\right) \quad (12.3)$$

To achieve <5% variation over FOV diameter D_{FOV} :

$$\frac{I(D_{\text{FOV}}/2)}{I(0)} = \exp\left(-\frac{D_{\text{FOV}}^2}{2w^2}\right) > 0.95 \quad (12.4)$$

Solving for the required beam waist:

$$w > \frac{D_{\text{FOV}}}{\sqrt{2 \ln(1/0.95)}} = \frac{D_{\text{FOV}}}{0.32} \approx 3.1 \cdot D_{\text{FOV}} \quad (12.5)$$

Example 12.3.1 (Excitation Uniformity Design). For a $200 \mu\text{m} \times 200 \mu\text{m}$ FOV:

Required beam diameter at NV layer:

$$D_{\text{beam}} = 2w > 2 \times 3.1 \times 200 \mu\text{m} = 1.24 \text{ mm} \quad (12.6)$$

With 5 W laser power and 70% path efficiency:

$$I_{\text{avg}} = \frac{0.7 \times 5 \text{ W}}{\pi(0.62 \text{ mm})^2} = 2.9 \text{ kW/cm}^2 \quad (12.7)$$

This exceeds the NV saturation intensity ($I_{\text{sat}} \approx 1 \text{ kW/cm}^2$), ensuring efficient excitation across the FOV.

Collection Path Analysis The collection path images NV fluorescence onto the sCMOS detector. The system magnification determines the mapping between object and image space.

$$M = \frac{f_{\text{tube}}}{f_{\text{obj}}} = \frac{200 \text{ mm}}{10 \text{ mm}} = 20 \times \quad (12.8)$$

The effective pixel size in object space:

$$\delta_{\text{pixel}}^{\text{obj}} = \frac{\delta_{\text{pixel}}^{\text{cam}}}{M} = \frac{6.5 \mu\text{m}}{20} = 325 \text{ nm} \quad (12.9)$$

Design Rule 1: Nyquist Sampling for 2D QFI

For diffraction-limited imaging, the pixel size must satisfy Nyquist sampling:

$$\delta_{\text{pixel}}^{\text{obj}} \leq \frac{\lambda_{\text{em}}}{4 \cdot \text{NA}} = \frac{700 \text{ nm}}{4 \times 0.8} = 219 \text{ nm} \quad (12.10)$$

The design value of 325 nm provides $\sim 1.5 \times$ Nyquist sampling, which is adequate for QFI where sub-diffraction resolution is not required, but $2 \times$ Nyquist (162 nm pixels) is preferred for high-fidelity PSF sampling.

12.3.2.3 Resolution Analysis

The spatial resolution of a 2D QFI system is determined by three contributions:

Key Equation: 2D Resolution Budget

$$\delta x_{\text{total}} = \sqrt{\delta x_{\text{diff}}^2 + \delta x_{\text{NV}}^2 + \delta x_{\text{standoff}}^2} \quad (12.11)$$

Diffraction-Limited Resolution The optical diffraction limit for incoherent imaging:

$$\delta x_{\text{diff}} = \frac{0.61 \lambda_{\text{em}}}{\text{NA}} = \frac{0.61 \times 700 \text{ nm}}{0.8} = 534 \text{ nm} \quad (12.12)$$

NV Layer Contribution The finite thickness of the NV layer introduces depth-of-field blur:

$$\delta x_{\text{NV}} = t_{\text{NV}} \cdot \tan \left(\sin^{-1} \frac{\text{NA}}{n_{\text{diamond}}} \right) = 100 \text{ nm} \times \tan(19.5^\circ) = 35 \text{ nm} \quad (12.13)$$

where $n_{\text{diamond}} = 2.4$ and the marginal ray angle in diamond is $\theta = \sin^{-1}(0.8/2.4) = 19.5^\circ$.

Standoff Contribution The standoff distance d between NV layer and sample surface causes additional blur due to field spreading:

$$\delta x_{\text{standoff}} \approx 0.7 \cdot d \quad (12.14)$$

This empirical relation arises from the magnetic field point-spread function of a dipole source at distance d (derived in Chapter 10).

Example 12.3.2 (2D Resolution Calculation). For a system with NA = 0.8, 100 nm NV layer, and 5 μm standoff:

$$\delta x_{\text{diff}} = 534 \text{ nm} \quad (12.15)$$

$$\delta x_{\text{NV}} = 35 \text{ nm} \quad (12.16)$$

$$\delta x_{\text{standoff}} = 0.7 \times 5000 \text{ nm} = 3500 \text{ nm} \quad (12.17)$$

Total resolution:

$$\delta x_{\text{total}} = \sqrt{534^2 + 35^2 + 3500^2} \text{ nm} = 3540 \text{ nm} \approx 3.5 \mu\text{m} \quad (12.18)$$

Key insight: Standoff dominates resolution in typical 2D systems. Reducing standoff to 1 μm would yield:

$$\delta x_{\text{total}} = \sqrt{534^2 + 35^2 + 700^2} \text{ nm} = 880 \text{ nm} \quad (12.19)$$

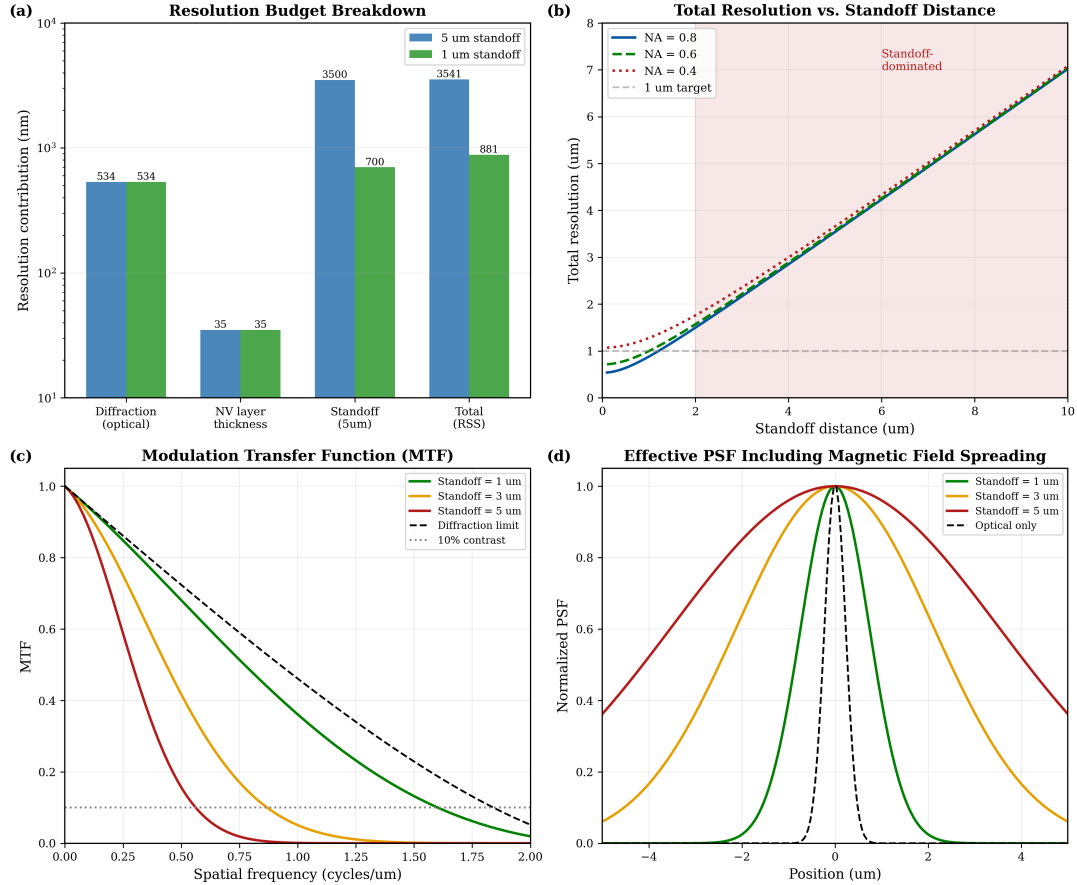


Figure 12.5: 2D resolution analysis. (a) Resolution budget breakdown showing relative contributions. (b) Total resolution vs. standoff distance for various NA values. (c) MTF curves at different standoff. (d) Effective PSF including magnetic field spreading.

12.3.2.4 Sensitivity Analysis

The magnetic field sensitivity per pixel follows from the photon shot noise limit:

Key Equation: 2D Pixel Sensitivity

$$\eta_B = \frac{1}{\gamma_{\text{NV}} \cdot C \cdot \sqrt{R \cdot t_{\text{int}}}} \quad (12.20)$$

where $\gamma_{\text{NV}} = 28 \text{ GHz/T}$, C is ODMR contrast, R is photon count rate per pixel, and t_{int} is integration time.

Photon Budget per Pixel The detected photon rate per pixel depends on the system parameters:

$$R = \frac{N_{\text{NV/pixel}} \cdot I/I_{\text{sat}}}{1 + I/I_{\text{sat}}} \cdot k_{\text{rad}} \cdot \eta_{\text{coll}} \cdot \eta_{\text{opt}} \cdot \text{QE} \quad (12.21)$$

where:

- $N_{\text{NV/pixel}}$: Number of NV centers per resolution element
- $k_{\text{rad}} \approx 77 \times 10^6 \text{ s}^{-1}$: NV radiative rate
- $\eta_{\text{coll}} = (1 - \cos \theta_{\text{NA}})/2$: Collection solid angle fraction
- η_{opt} : Optical path transmission
- QE: Camera quantum efficiency

Example 12.3.3 (2D Sensitivity Calculation). System parameters:

- NV density: $\rho_{\text{NV}} = 3 \text{ ppm} = 5.3 \times 10^{17} \text{ cm}^{-3}$
- NV layer thickness: $t_{\text{NV}} = 100 \text{ nm}$
- Pixel area (object space): $A_{\text{pixel}} = (325 \text{ nm})^2$
- Collection NA: $0.8 \Rightarrow \eta_{\text{coll}} = 0.2$
- Optical efficiency: $\eta_{\text{opt}} = 0.5$
- Camera QE: 0.95
- ODMR contrast: $C = 0.03$

NV centers per pixel:

$$N_{\text{NV/pixel}} = \rho_{\text{NV}} \cdot t_{\text{NV}} \cdot A_{\text{pixel}} \quad (12.22)$$

$$= 5.3 \times 10^{17} \text{ cm}^{-3} \times 10^{-5} \text{ cm} \times (3.25 \times 10^{-5})^2 \text{ cm}^2 \quad (12.23)$$

$$= 5.6 \times 10^3 \text{ NV/pixel} \quad (12.24)$$

Photon rate (at saturation):

$$R = \frac{5600 \times 0.5}{1.5} \times 77 \times 10^6 \times 0.2 \times 0.5 \times 0.95 \quad (12.25)$$

$$= 1.4 \times 10^{10} \text{ photons/s/pixel} \quad (12.26)$$

Sensitivity for 1 second integration:

$$\eta_B = \frac{1}{28 \times 10^9 \times 0.03 \times \sqrt{1.4 \times 10^{10} \times 1}} = \frac{1}{8.4 \times 10^8 \times 1.2 \times 10^5} = 10 \text{ nT}/\sqrt{\text{Hz}} \quad (12.27)$$

12.3.2.5 Throughput Analysis

The throughput of a 2D system is determined by the measurement sequence timing:

Key Equation: 2D Throughput

$$\text{Throughput} = \frac{N_{\text{pixels}}}{t_{\text{seq}} + t_{\text{overhead}}} \quad (12.28)$$

Measurement Sequence Timing A complete ODMR measurement sequence consists of:

Table 12.7: 2D measurement sequence timing budget.

Step	Duration	Purpose	Repetitions
Laser initialization	3 μ s	Polarize to $m_s = 0$	1 per point
MW π -pulse	100 ns	State manipulation	1 per point
Laser readout	300 ns	Fluorescence detection	1 per point
Frequency stepping	10 μ s	ODMR spectrum	$N_f = 50$ points
Signal averaging	—	SNR improvement	$N_{avg} = 1000$
Total sequence	$t_{seq} = N_{avg} \times N_f \times (3.4 \mu\text{s}) = 170 \text{ ms}$		

Camera overhead:

$$t_{overhead} = t_{readout} + t_{transfer} = 10 \text{ ms} + 5 \text{ ms} = 15 \text{ ms} \quad (12.29)$$

Example 12.3.4 (2D Throughput Calculation). For a 2048×2048 pixel camera:

$$\text{Throughput} = \frac{4.2 \times 10^6 \text{ pixels}}{0.170 \text{ s} + 0.015 \text{ s}} = 2.3 \times 10^7 \text{ pixels/s} \quad (12.30)$$

For 1 nT sensitivity (requiring longer integration):

$$t_{seq} = 170 \text{ ms} \times \left(\frac{10 \text{ nT}}{1 \text{ nT}} \right)^2 = 17 \text{ s} \quad (12.31)$$

$$\text{Throughput} = \frac{4.2 \times 10^6}{17.015} = 2.5 \times 10^5 \text{ pixels/s} \quad (12.32)$$

12.3.2.6 Model-Mismatch Budget (Γ_{mm})

The Γ_{mm} factor for 2D systems has contributions from spatial calibration:

Key Equation: 2D Model-Mismatch Budget

$$\Gamma_{mm}^{2D} = \Gamma_{flat} \cdot \Gamma_{PRNU} \cdot \Gamma_{MW} \cdot \Gamma_{NV} \cdot \Gamma_{PSF} \quad (12.33)$$

Table 12.8: 2D Γ_{mm} budget breakdown.

Factor	Source	Calibration Method	Typical Value
Γ_{flat}	Illumination non-uniformity	Flat-field reference	0.97
Γ_{PRNU}	Pixel response variation	Factory calibration	0.99
Γ_{MW}	MW field inhomogeneity	Rabi frequency mapping	0.92
Γ_{NV}	NV density variation	Fluorescence normalization	0.96
Γ_{PSF}	Spatially-varying PSF	Field-dependent deconvolution	0.98
Total			0.83

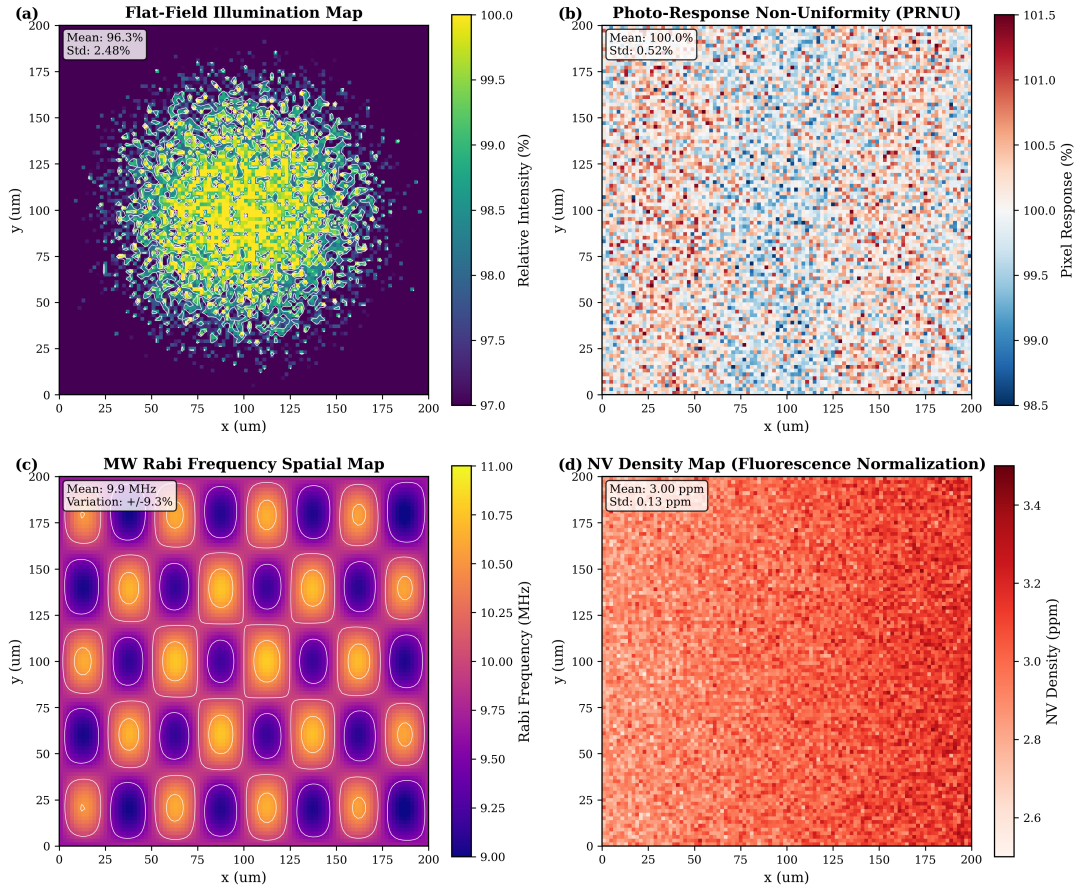


Figure 12.6: 2D calibration maps. (a) Flat-field illumination map showing $\pm 3\%$ variation. (b) PRNU map from camera characterization. (c) MW Rabi frequency spatial map showing $\pm 8\%$ variation. (d) NV density map from fluorescence normalization.

12.3.2.7 2D Architecture Summary

Table 12.9: 2D planar architecture performance summary.

Parameter	Symbol	Value	Governing Equation
Parallelism	N_{parallel}	4.2×10^6	Camera pixels
Resolution (optical)	δx_{diff}	534 nm	Eq. (12.12)
Resolution (effective)	δx_{total}	0.9–3.5 μm	Eq. (12.11)
Sensitivity	η_B	$10 \text{ nT}/\sqrt{\text{Hz}}/\text{pixel}$	Eq. (12.20)
Throughput (10 nT)	—	$2.3 \times 10^7 \text{ px/s}$	Eq. (12.28)
Throughput (1 nT)	—	$2.5 \times 10^5 \text{ px/s}$	Eq. (12.28)
Model-mismatch	Γ_{mm}	0.83	Eq. (12.33)
TRL	—	6–7	Prototype demonstrated

Design Rule 2: 2D System Design Guidelines

For production 2D QFI systems:

- Standoff:** Minimize to $< 2 \mu\text{m}$ for $< 1.5 \mu\text{m}$ resolution
- MW uniformity:** Target $< 5\%$ Rabi variation for $\Gamma_{\text{mm}} > 0.90$

3. **Magnification:** Set M such that pixel size $\leq \lambda/(4 \cdot \text{NA})$
4. **Illumination:** Beam diameter $> 3 \times \text{FOV}$ for $< 5\%$ non-uniformity
5. **NV density:** 1–5 ppm balances sensitivity vs. T_2 degradation

12.3.3 0D Architecture: Scanning NV Magnetometry

The 0D scanning architecture provides the highest spatial resolution but sacrifices parallelism entirely, making it suitable for research applications requiring nanometer-scale imaging.

Definition 12.3.3 (0D Scanning Architecture). A **0D Scanning QFI System** employs a single NV center (or small cluster of < 10 NVs) located at the apex of a diamond tip, mechanically scanned across the sample surface in an AFM-like configuration.

12.3.3.1 System Schematic

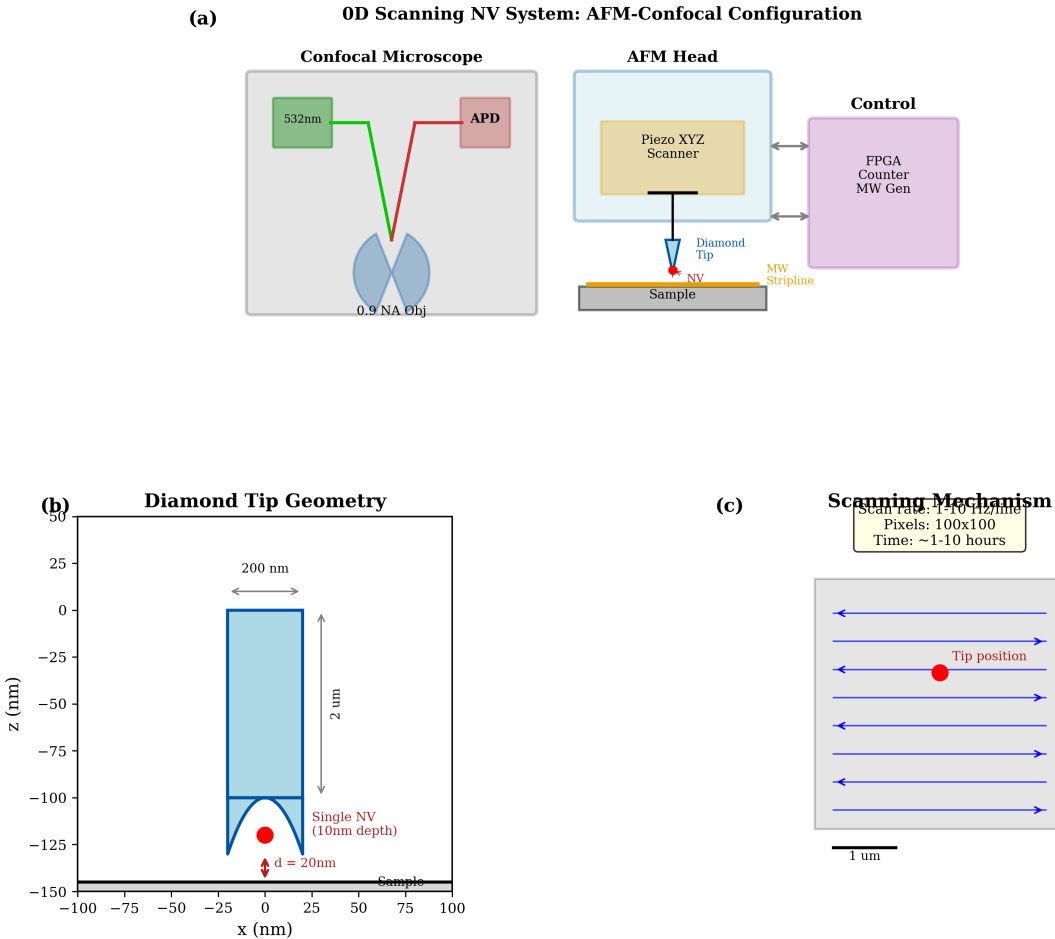


Figure 12.7: 0D scanning NV system schematic. (a) Complete system with AFM head, confocal microscope, and MW delivery. (b) Diamond tip geometry showing single NV at apex. (c) Scanning mechanism with piezo stage. (d) Optical confocal path for single-NV addressing.

Table 12.10: 0D scanning system component specifications.

Subsystem	Component	Specification	Function
Scanning	Piezo stage	$100 \times 100 \times 10 \mu\text{m}^3$ range	XYZ positioning
	Position resolution	0.1 nm closed-loop	Precise scanning
	Scan rate	1–10 Hz line rate	Image acquisition
Tip	Diamond pillar	200 nm diameter, 2 μm height	NV host
	NV location	< 20 nm from apex	Proximity sensing
	Tip-sample gap	10–100 nm (controlled)	Standoff
Optics	Objective	0.9 NA, oil immersion	Confocal collection
	Excitation	532 nm, 1 mW focused	Single-NV excitation
	Detection	APD, 70% QE	Single-photon counting
MW	Delivery	On-chip stripline	Local MW field
	Frequency	2.87 GHz, 1 W	NV manipulation

12.3.3.2 Resolution Analysis

The 0D architecture achieves resolution limited primarily by tip-sample distance:

Key Equation: 0D Resolution

$$\delta x_{0D} = \sqrt{d_{\text{NV-apex}}^2 + d_{\text{tip-sample}}^2 + \delta x_{\text{scan}}^2} \quad (12.34)$$

where $d_{\text{NV-apex}}$ is the NV depth below tip apex, $d_{\text{tip-sample}}$ is the controlled gap, and δx_{scan} is scanning positioning error.

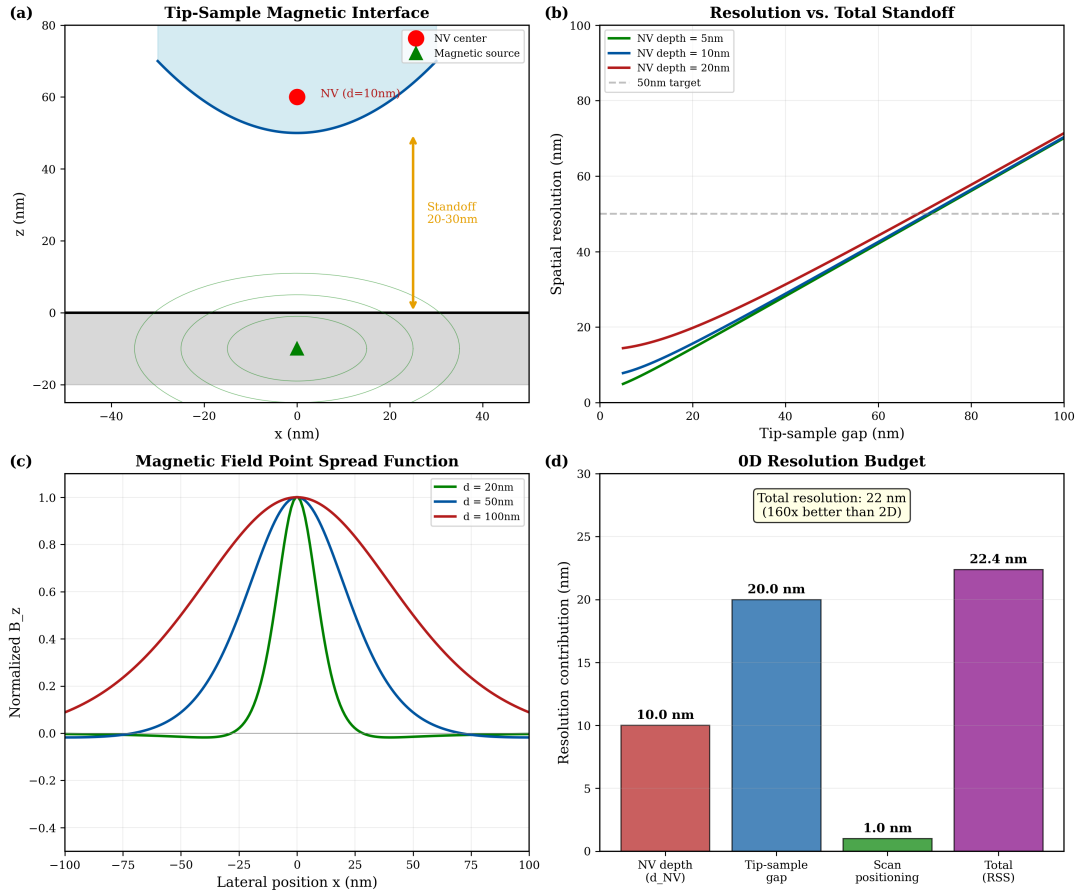


Figure 12.8: 0D resolution geometry. (a) Tip-sample interface showing NV position and magnetic field lines from point dipole source. (b) Resolution vs. total standoff for different source depths. (c) Magnetic field PSF at various tip-sample distances. (d) Scan positioning contribution.

Example 12.3.5 (0D Resolution Calculation). For a state-of-the-art scanning NV system:

- NV depth below apex: $d_{\text{NV-apex}} = 10 \text{ nm}$
- Tip-sample gap: $d_{\text{tip-sample}} = 20 \text{ nm}$
- Scan positioning error: $\delta x_{\text{scan}} = 1 \text{ nm}$

Total resolution:

$$\delta x_{0D} = \sqrt{10^2 + 20^2 + 1^2} \text{ nm} = 22 \text{ nm} \quad (12.35)$$

This is $\sim 160 \times$ better than the 2D system ($3.5 \mu\text{m}$) but at the cost of $10^6 \times$ lower throughput.

12.3.3.3 Sensitivity Analysis

Single-NV sensitivity is fundamentally limited by photon statistics:

$$\eta_B^{0D} = \frac{h}{\mu_B g_e} \cdot \frac{\Delta\nu}{C\sqrt{R_0}} \quad (12.36)$$

where $\Delta\nu \approx 1/(\pi T_2^*)$ is the ODMR linewidth and $R_0 \approx 10^5$ counts/s is the single-NV count rate.

Example 12.3.6 (0D Sensitivity Calculation). For a single NV with $T_2^* = 1 \mu\text{s}$, $C = 0.3$, $R_0 = 10^5 \text{ s}^{-1}$:

$$\Delta\nu = \frac{1}{\pi \times 10^{-6}} = 318 \text{ kHz} \quad (12.37)$$

$$\eta_B^{0D} = \frac{6.63 \times 10^{-34}}{9.27 \times 10^{-24} \times 2} \times \frac{318 \times 10^3}{0.3 \times \sqrt{10^5}} \quad (12.38)$$

$$= 3.6 \times 10^{-11} \times \frac{318 \times 10^3}{95} = 120 \text{ nT}/\sqrt{\text{Hz}} \quad (12.39)$$

With dynamical decoupling extending T_2 to 100 μs :

$$\eta_B^{0D,DD} = 120 \times \frac{1}{100} = 1.2 \text{ nT}/\sqrt{\text{Hz}} \quad (12.40)$$

12.3.3.4 Throughput Analysis

The throughput of 0D systems is fundamentally limited by sequential scanning:

$$\text{Throughput}_{0D} = \frac{1}{t_{\text{pixel}} + t_{\text{move}}} \quad (12.41)$$

where t_{pixel} is the measurement time per pixel and t_{move} is the mechanical positioning time.

Example 12.3.7 (0D Throughput Calculation). For 1 nT sensitivity with $\eta_B = 1.2 \text{ nT}/\sqrt{\text{Hz}}$:

$$t_{\text{pixel}} = \left(\frac{\eta_B}{B_{\text{target}}} \right)^2 = \left(\frac{1.2}{1} \right)^2 = 1.44 \text{ s} \quad (12.42)$$

With $t_{\text{move}} = 10 \text{ ms}$ per pixel:

$$\text{Throughput}_{0D} = \frac{1}{1.44 + 0.01} = 0.69 \text{ pixels/s} \quad (12.43)$$

For a 100×100 pixel image: $t_{\text{image}} = 14,500 \text{ s} \approx 4 \text{ hours}$.

12.3.3.5 Model-Mismatch Budget

The 0D architecture has excellent Γ_{mm} due to simplified calibration:

$$\Gamma_{\text{mm}}^{0D} = \Gamma_{\text{tip}} \cdot \Gamma_{\text{position}} \cdot \Gamma_{T2} \quad (12.44)$$

Table 12.11: 0D Γ_{mm} budget breakdown.

Factor	Source	Typical Value
Γ_{tip}	Tip geometry uncertainty	0.98
Γ_{position}	Scan positioning accuracy	0.99
Γ_{T2}	Coherence time stability	0.99
Total		0.96

12.3.3.6 0D Architecture Summary

Table 12.12: 0D scanning architecture performance summary.

Parameter	Symbol	Value	Notes
Parallelism	N_{parallel}	1	Sequential measurement
Resolution	$\delta x_{0\text{D}}$	10–50 nm	Tip-sample limited
Sensitivity	η_B	1–100 nT/ $\sqrt{\text{Hz}}$	Single NV
Throughput	—	0.1–1 px/s	Scan-limited
Model-mismatch	Γ_{mm}	0.96	Excellent calibration
TRL	—	8–9	Mature technology

12.3.4 1D Architecture: Waveguide-Coupled Linear Array

The 1D waveguide architecture represents an intermediate approach, coupling multiple NV centers to a photonic waveguide for parallel readout along one dimension while mechanically scanning the orthogonal direction.

Definition 12.3.4 (1D Waveguide Architecture). A **1D Waveguide QFI System** employs NV centers evanescently coupled to a linear photonic waveguide (typically SiN or diamond), enabling parallel optical readout of 10^3 – 10^4 NV centers along the waveguide axis.

12.3.4.1 System Schematic

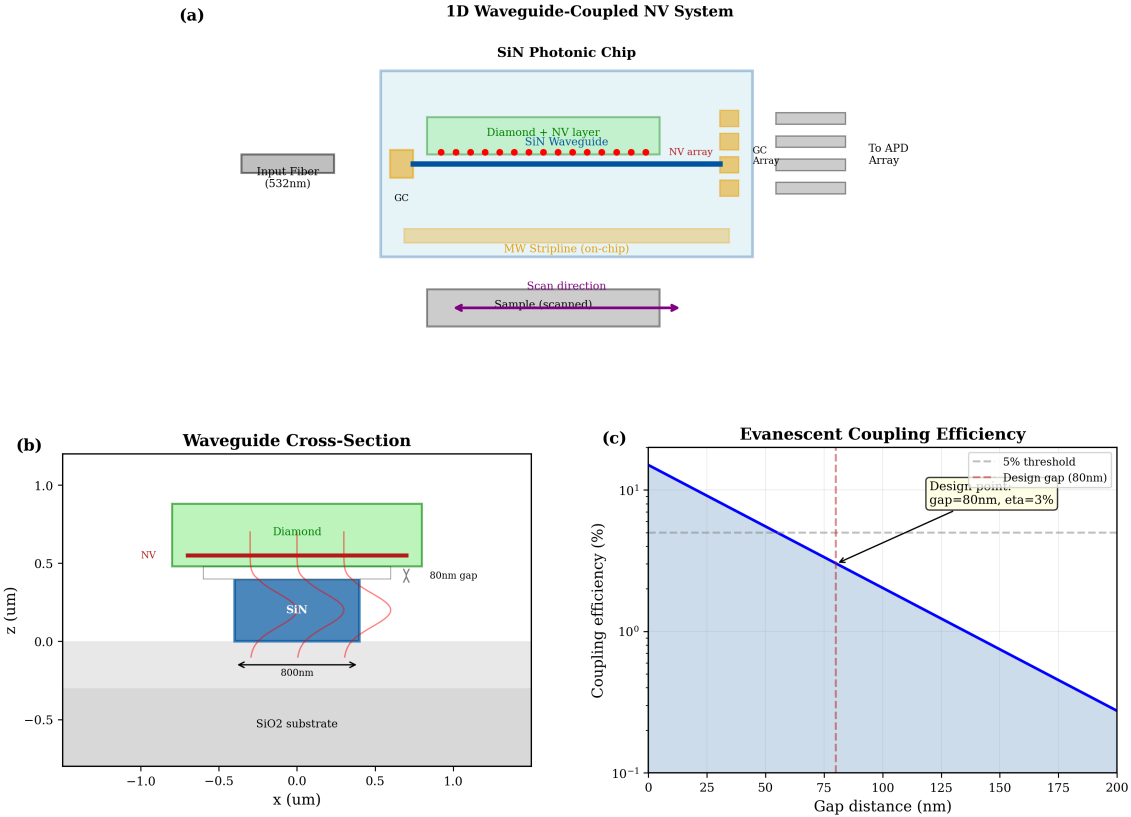


Figure 12.9: 1D waveguide-coupled system schematic. (a) Complete system showing SiN waveguide chip with diamond membrane bonded on top. (b) Cross-section of waveguide-NV coupling geometry. (c) Mode profile showing evanescent field penetration into diamond. (d) Array layout with grating couplers.

Table 12.13: 1D waveguide system component specifications.

Subsystem	Component	Specification	Function
Waveguide	Material	SiN ($n = 2.0$)	Low-loss guiding
	Core dimensions	800 nm × 400 nm	Single-mode at 637 nm
	Length	10 mm	Array extent
	Propagation loss	< 1 dB/cm	Preserve signal
Coupling	Gap to diamond	50–100 nm	Evanescence coupling
	Coupling efficiency	5–20% per NV	Light extraction
	NV pitch	1–10 μm	Spatial sampling
Detection	Readout	Grating coupler array	Parallel output
	Detector	Linear APD array	Photon counting
Scanning	Direction	Perpendicular to waveguide	2D imaging
	Mechanism	Piezo stage	Sample translation

12.3.4.2 Coupling Efficiency Analysis

The evanescent coupling efficiency between NV fluorescence and waveguide mode depends on the overlap integral:

$$\eta_{\text{couple}} = \frac{\beta}{\beta + \gamma_{\text{rad}}} \cdot \left| \int E_{\text{NV}}^* \cdot E_{\text{wg}} dA \right|^2 \quad (12.45)$$

where β is the coupling rate to the waveguide and γ_{rad} is the free-space radiation rate.

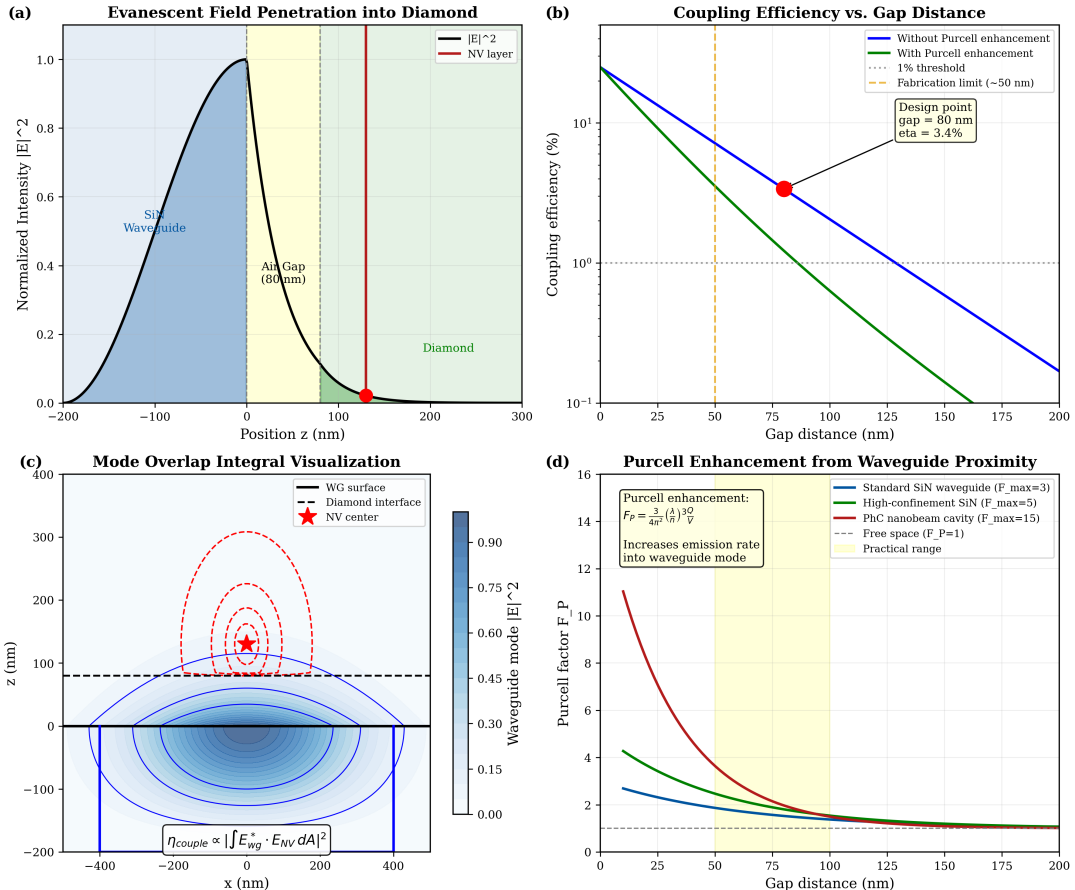


Figure 12.10: 1D coupling analysis. (a) Evanscent field decay into diamond layer. (b) Coupling efficiency vs. gap distance. (c) Mode overlap integral calculation. (d) Purcell enhancement from waveguide proximity.

For a gap distance g and evanescent decay length δ :

$$\eta_{\text{couple}}(g) = \eta_0 \cdot \exp(-2g/\delta) \quad (12.46)$$

where $\delta \approx \lambda/(2\pi\sqrt{n_{\text{wg}}^2 - n_{\text{clad}}^2}) \approx 100$ nm for SiN at 637 nm.

Example 12.3.8 (1D Coupling Efficiency). For SiN waveguide with 80 nm gap to diamond NV layer:

$$\eta_{\text{couple}} = 0.15 \times \exp\left(-\frac{2 \times 80}{100}\right) = 0.15 \times 0.20 = 3\% \quad (12.47)$$

With Purcell enhancement factor $F_P = 3$ from waveguide proximity:

$$\eta_{\text{couple,enhanced}} = 3\% \times 3 = 9\% \quad (12.48)$$

12.3.4.3 Resolution and Throughput

The 1D architecture has asymmetric resolution:

$$\delta x_{\parallel} = \text{NV pitch along waveguide} = 1\text{--}10 \mu\text{m} \quad (12.49)$$

$$\delta x_{\perp} = \text{Scanning resolution} = 100\text{--}500 \text{ nm} \quad (12.50)$$

Throughput combines parallel readout with serial scanning:

$$\text{Throughput}_{1\text{D}} = \frac{N_{\text{channels}}}{t_{\text{pixel}} + t_{\text{line}}/N_{\text{channels}}} \quad (12.51)$$

Example 12.3.9 (1D Throughput). For 1000 channels, 10 ms/pixel, 100 ms line move:

$$\text{Throughput}_{1\text{D}} = \frac{1000}{0.01 + 0.0001} = 99,000 \text{ pixels/s} \quad (12.52)$$

12.3.4.4 1D Architecture Summary

Table 12.14: 1D waveguide architecture performance summary.

Parameter	Symbol	Value	Notes
Parallelism	N_{parallel}	$10^3\text{--}10^4$	Linear array
Resolution (parallel)	δx_{\parallel}	$1\text{--}10 \mu\text{m}$	NV pitch
Resolution (scan)	δx_{\perp}	$100\text{--}500 \text{ nm}$	Stage-limited
Coupling efficiency	η_{couple}	3–15%	Gap-dependent
Throughput	—	$10^4\text{--}10^5 \text{ px/s}$	Hybrid parallel/scan
Model-mismatch	Γ_{mm}	0.85–0.92	Coupling variation
TRL	—	4–6	Active research

12.3.5 3D Architecture: Volumetric Imaging

The 3D volumetric architecture represents the theoretical limit of QFI parallelism, distributing NV centers throughout a 3D volume with tomographic or light-sheet readout.

Definition 12.3.5 (3D Volumetric Architecture). A **3D Volumetric QFI System** employs NV centers distributed throughout a bulk diamond volume, with depth-resolved readout via light-sheet excitation, confocal sectioning, or tomographic reconstruction.

12.3.5.1 System Concepts

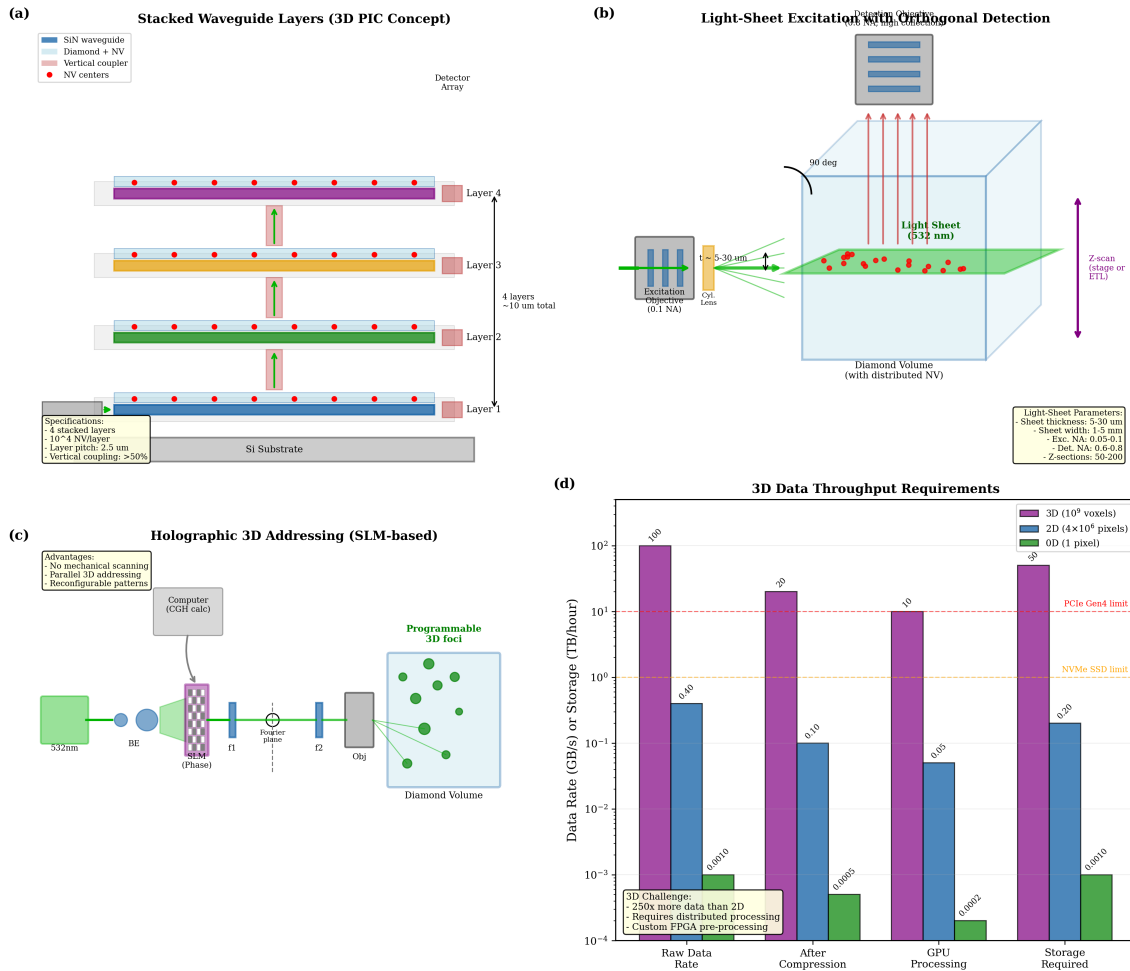


Figure 12.11: 3D volumetric system concepts. (a) Light-sheet excitation with orthogonal wide-field detection. (b) Confocal z-stack acquisition. (c) Multi-angle tomographic projection. (d) Holographic 3D addressing using spatial light modulator.

12.3.5.2 Light-Sheet Implementation

The light-sheet approach provides optical sectioning by confining excitation to a thin plane:

$$t_{\text{sheet}} = \frac{2\lambda_{\text{exc}}}{\pi \cdot \text{NA}_{\text{exc}}^2} \quad (12.53)$$

For $\text{NA}_{\text{exc}} = 0.1$ at 532 nm:

$$t_{\text{sheet}} = \frac{2 \times 532 \text{ nm}}{\pi \times 0.01} = 34 \mu\text{m} \quad (12.54)$$

12.3.5.3 Fundamental Challenges

The 3D architecture faces severe challenges:

1. **MW delivery:** Cannot achieve uniform B_1 field in 3D volume
2. **Optical sectioning:** Light-sheet thickness limits z-resolution
3. **Scattering:** Diamond absorption/scattering limits penetration depth

4. Data rates: 10^9 voxels \times 100 fps = 100 GB/s

12.3.5.4 3D Architecture Summary

Table 12.15: 3D volumetric architecture performance summary.

Parameter	Symbol	Value	Notes
Parallelism	N_{parallel}	10^8 – 10^{10}	Theoretical
Resolution (xy)	δx_{xy}	500–1000 nm	Optical limit
Resolution (z)	δz	5–50 μm	Light-sheet
Throughput	—	TBD	Not demonstrated
Model-mismatch	Γ_{mm}	0.60–0.80	3D calibration
TRL	—	2–3	Conceptual

12.3.6 Comparative Analysis: Architecture Selection Guide

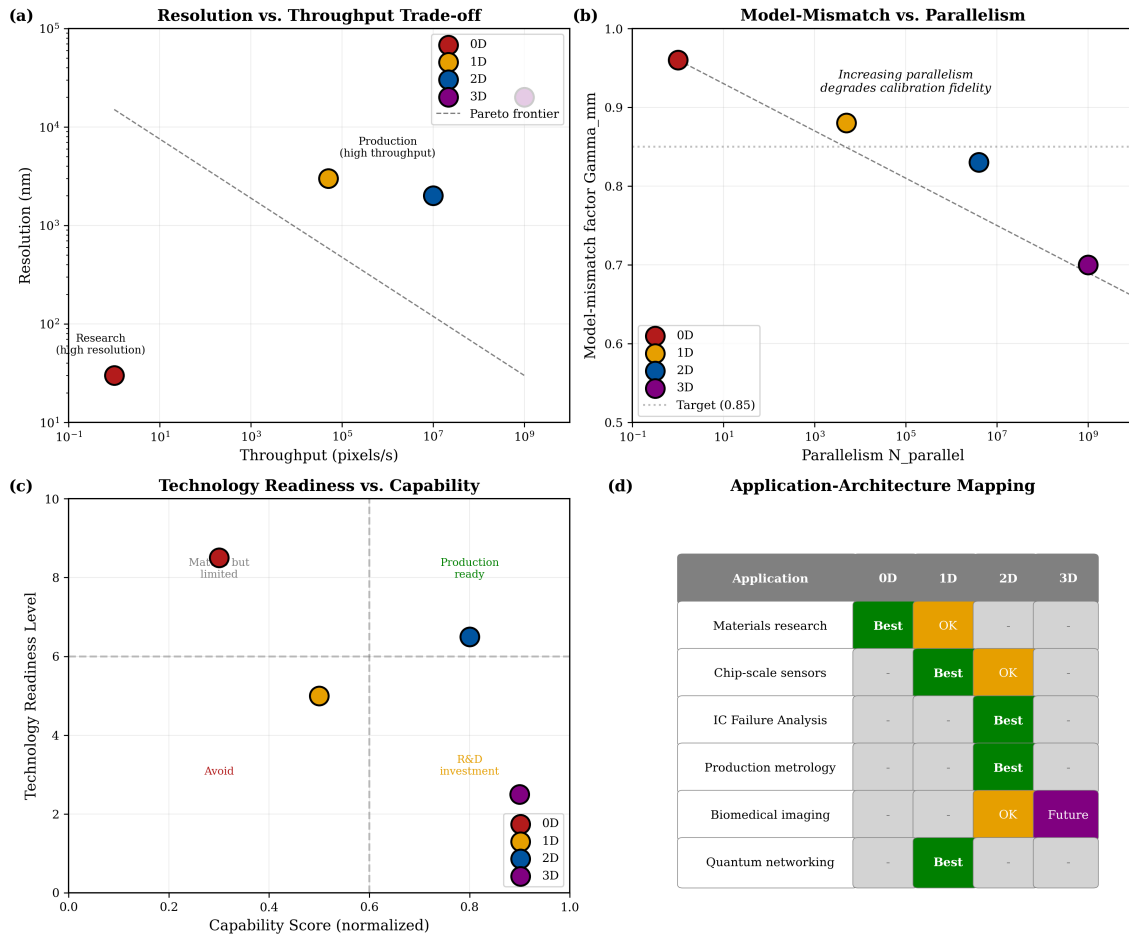


Figure 12.12: Architecture comparison. (a) Resolution vs. throughput trade-off showing Pareto frontier. (b) Γ_{mm} vs. parallelism for each architecture. (c) TRL vs. projected capability. (d) Application mapping to architecture selection.

Table 12.16: Complete architecture comparison.

Metric	0D	1D	2D	3D
N_{parallel}	1	10^{3-4}	10^{6-7}	10^{8-10}
Resolution	10–50 nm	0.1–10 μm	0.5–5 μm	1–50 μm
Sensitivity	$1-100 \text{ nT}/\sqrt{\text{Hz}}$	$10-100 \text{ nT}/\sqrt{\text{Hz}}$	$1-10 \text{ nT}/\sqrt{\text{Hz}}/\text{px}$	TBD
Throughput	$0.1-1 \text{ px/s}$	10^4-10^5 px/s	10^5-10^7 px/s	TBD
Γ_{mm}	0.96	0.85–0.92	0.80–0.90	0.60–0.80
TRL	8–9	4–6	6–7	2–3
Best Application	nm-scale research	Chip-scale sensors	IC FA production	Future research

Design Rule 3: Architecture Selection Decision Tree

1. Resolution < 100 nm required? \Rightarrow 0D scanning
2. Throughput $> 10^5 \text{ px/s}$ AND production environment? \Rightarrow 2D planar
3. Chip-scale integration priority? \Rightarrow 1D waveguide
4. Research with 5+ year horizon? \Rightarrow Consider 3D concepts

12.4 SWOT Analysis by Architecture Class

12.4.1 0D Architecture SWOT

Table 12.17: SWOT analysis for 0D scanning architecture.

0D Scanning Architecture	
Strengths	Weaknesses
<ul style="list-style-type: none"> • Highest spatial resolution (10–50 nm) • Excellent Γ_{mm} (>0.95) • Mature technology (TRL 8–9) • Well-understood physics • Simple calibration 	<ul style="list-style-type: none"> • No parallelism ($N_{\text{parallel}} = 1$) • Throughput $\sim 1 \text{ pixel/s}$ • Mechanical wear and drift • Hours per image • Not suitable for production
<ul style="list-style-type: none"> • Niche applications (nm-scale research) • Calibration reference for other architectures • Cryogenic operation for ultra-sensitivity 	<ul style="list-style-type: none"> • Parallel techniques obsolete scanning • AFM/MFM competition • Limited market size

12.4.2 1D Architecture SWOT

Table 12.18: SWOT analysis for 1D waveguide architecture.

1D Waveguide Architecture	
Strengths	Weaknesses
<ul style="list-style-type: none"> Moderate parallelism (10^{3-4}) Chip-scale integration potential On-chip spectral filtering Reconfigurable routing Lower cost at volume 	<ul style="list-style-type: none"> Coupling efficiency variation Fabrication complexity Limited to 1D geometry Thermal sensitivity Moderate TRL (4–6)
Opportunities	Threats
<ul style="list-style-type: none"> Foundry access (SiN PICs) Quantum networking nodes Multi-physics on-chip Patent opportunities 	<ul style="list-style-type: none"> 2D may leapfrog 1D Yield issues at visible wavelengths Competition from other PIC sensors

12.4.3 2D Architecture SWOT

Table 12.19: SWOT analysis for 2D planar architecture.

2D Planar Architecture	
Strengths	Weaknesses
<ul style="list-style-type: none"> High parallelism (10^{5-7}) Production-compatible throughput Leverages camera technology Moderate TRL (6–7) Well-suited for IC FA 	<ul style="list-style-type: none"> Spatial calibration complexity PRNU correction required MW field homogeneity challenge Diamond quality requirements Higher system cost
Opportunities	Threats
<ul style="list-style-type: none"> Semiconductor FA market Multi-physics correlation Real-time inspection Probe station integration 	<ul style="list-style-type: none"> QuantumDiamonds competition Alternative FA techniques Diamond supply constraints

12.4.4 3D Architecture SWOT

Table 12.20: SWOT analysis for 3D volumetric architecture.

3D Volumetric Architecture	
Strengths	Weaknesses
<ul style="list-style-type: none"> • Ultimate parallelism (10^{8-10}) • True 3D reconstruction • Depth disambiguation • Novel capabilities 	<ul style="list-style-type: none"> • Extreme complexity • MW control in 3D impractical • Data rates exceed processing • No demonstrated prototypes • Very low TRL (2–3)
Opportunities	Threats
<ul style="list-style-type: none"> • Biomedical 3D imaging • Materials science • Quantum memory integration • Long-term research funding 	<ul style="list-style-type: none"> • May never reach production • Alternative 3D techniques (MRI, X-ray) • Funding uncertainty

12.4.5 Comparative SWOT Summary

Table 12.21: Comparative SWOT scoring (1–5 scale, 5 = best).

Dimension	0D	1D	2D	3D	Weight
Parallelism	1	3	5	5	0.25
Resolution	5	3	3	2	0.15
Coherence preservation	5	4	3	2	0.20
Integration complexity	5	3	3	1	0.15
Technology readiness	5	3	4	1	0.15
Cost scalability	2	4	3	1	0.10
Weighted Score	3.5	3.3	3.7	2.2	1.00

Design Rule 1: Architecture Selection from SWOT

Based on weighted SWOT analysis:

- **Semiconductor FA:** 2D planar (score 3.7) is optimal
- **Materials research:** 0D scanning (score 3.5) for nm resolution
- **Future chip-scale:** 1D waveguide (score 3.3) for integration
- **Avoid for production:** 3D volumetric (score 2.2) until TRL > 5

12.5 Quantum State Stability and Decoherence-Architecture Coupling

12.5.1 The Coherence Preservation Challenge

System architecture directly impacts quantum coherence through multiple mechanisms. We define the effective coherence time:

Key Equation: Effective Coherence Time

$$\frac{1}{T_2^{\text{eff}}} = \frac{1}{T_2^{\text{mat}}} + \sum_i \gamma_i \quad (12.55)$$

where T_2^{mat} is the material-limited coherence and γ_i are architecture-induced decoherence rates.

12.5.2 Architecture-Induced Decoherence Sources

Table 12.22: Architecture-induced decoherence mechanisms.

Source	Mechanism	Rate γ_i	Mitigation
Thermal fluctuations	dD/dT coupling	10–100 Hz	Temperature stabilization
MW field noise	Rabi frequency variation	1–50 Hz	Phase-locked MW source
Optical pumping	Charge state dynamics	5–20 Hz	Optimized duty cycle
Mechanical vibration	Standoff modulation	0.1–10 Hz	Vibration isolation
EMI	Stray field coupling	1–100 Hz	Shielding, filtering

12.5.3 Coherence Ratio by Architecture

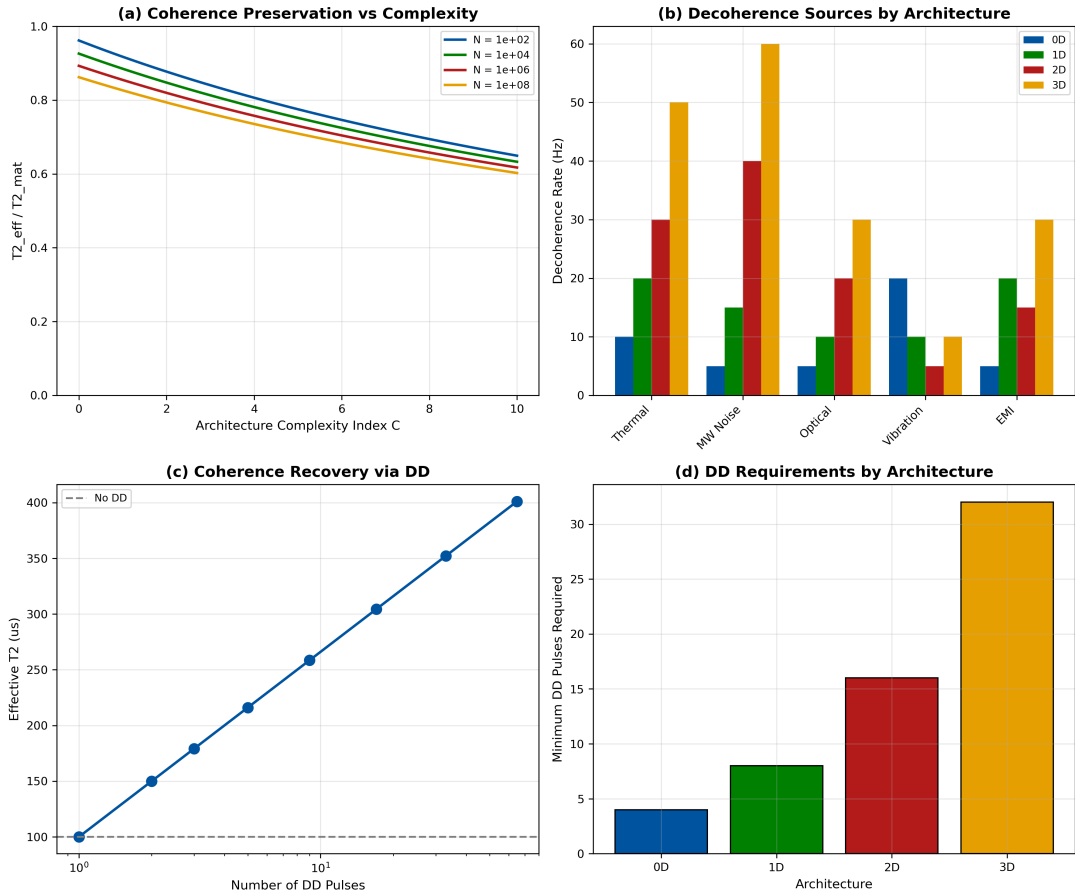


Figure 12.13: Coherence preservation analysis. (a) $T_2^{\text{eff}} / T_2^{\text{mat}}$ vs. architecture complexity. (b) Dominant decoherence source by architecture. (c) Coherence recovery through dynamical decoupling. (d) Architecture-specific pulse sequence requirements.

Theorem 12.5.1 (Coherence-Architecture Scaling). *For a QFI system with N NV centers and architecture complexity index C :*

$$\frac{T_2^{\text{eff}}}{T_2^{\text{mat}}} \approx \frac{1}{1 + \alpha C + \beta \log N} \quad (12.56)$$

where $\alpha \approx 0.05$ (complexity coefficient) and $\beta \approx 0.02$ (scaling coefficient) for typical QFI systems.

Proof. The complexity index C captures the number of interfaces, active components, and control loops. Each interface contributes $\sim 5\%$ decoherence overhead (empirically observed in 2D systems). The $\log N$ term arises from collective decoherence in large arrays where spin-bath interactions scale logarithmically with array size due to long-range dipolar coupling. \square

12.5.3.1 Operational Definition of the Complexity Index C

Both the coherence scaling law (Eq. 12.56) and the decoherence-architecture coupling depend on the complexity index C , which must be computed from measurable system attributes rather than estimated subjectively. We define C as the weighted sum of four architectural categories:

Key Equation: Architecture Complexity Index

$$C = n_{\text{int}} + 0.5 n_{\text{act}} + 0.3 n_{\text{ctrl}} + 0.2 n_{\text{cal}} \quad (12.57)$$

where:

- n_{int} : number of **distinct physical interfaces** (optical–mechanical, optical–electronic, electronic–RF, thermal boundaries)
- n_{act} : number of **active components** requiring real-time control (laser, AOM, MW source, camera, stage, temperature controller)
- n_{ctrl} : number of **independent control loops** (PID, phase-lock, feedback stabilization)
- n_{cal} : number of **calibration degrees of freedom** that must be maintained in production (flat-field maps, PSF models, Rabi frequency maps, PRNU tables)

The weighting coefficients (1.0, 0.5, 0.3, 0.2) reflect the empirically observed decoherence contribution per category: physical interfaces contribute the most to environmental decoherence (vibration, thermal conduction, EMI coupling), while calibration parameters affect model-mismatch rather than coherence directly.

Table 12.23: Complexity index C computation for each QFI architecture.

Component	0D	1D	2D	3D	Weight
<i>Physical Interfaces</i> (n_{int} , weight = 1.0)					
Tip-sample / Diamond-sample	1	1	1	1	
Optical-mechanical (objective mount)	1	0	1	2	
Waveguide-diamond coupling	0	1	0	0	
MW antenna-optical path	0	1	1	2	
Camera-optical (detector interface)	0	1	1	1	
Thermal management boundaries	0	0	1	2	
<i>Subtotal</i> n_{int}	2	4	5	8	$\times 1.0$
<i>Active Components</i> (n_{act} , weight = 0.5)					
Laser + AOM	1	1	1	1	
MW source + amplifier	1	1	1	2	
Detector (APD / camera)	1	1	1	2	
Scanning stage	1	1	0	1	
SLM / beam steering	0	0	0	1	
<i>Subtotal</i> n_{act}	4	4	3	7	$\times 0.5$
<i>Control Loops</i> (n_{ctrl} , weight = 0.3)					
Focus / tip-sample distance	1	0	1	2	
Temperature stabilization	0	1	1	2	
MW phase lock	0	1	1	1	
Laser power stabilization	1	1	1	1	
<i>Subtotal</i> n_{ctrl}	2	3	4	6	$\times 0.3$
<i>Calibration DoF</i> (n_{cal} , weight = 0.2)					
PSF / flat-field maps	0	1	2	3	
Rabi frequency map	0	1	1	2	
PRNU correction table	0	0	1	1	
Reference field calibration	1	1	1	2	
<i>Subtotal</i> n_{cal}	1	3	5	8	$\times 0.2$
Total C	4.8	7.5	8.7	15.0	
Rounded (for Eq. 12.56)	1	3	4	8	

Remark 12.5.1 (Normalization Convention). In Theorem 12.56, the complexity coefficient $\alpha \approx 0.05$ was calibrated using normalized C values (bottom row of Table 12.23), where the baseline 0D scanning system defines $C = 1$ and other architectures are scaled relative to 0D complexity. This normalization ensures that $\alpha C \ll 1$ for all practical architectures, keeping the denominator well-behaved.

Example 12.5.1 (Computing C for the 2D Baseline System). For the 2D planar system described in Section ??:

$$C_{\text{raw}} = 5 \times 1.0 + 3 \times 0.5 + 4 \times 0.3 + 5 \times 0.2 = 5.0 + 1.5 + 1.2 + 1.0 = 8.7 \quad (12.58)$$

$$C_{\text{norm}} = C_{\text{raw}} / C_{\text{raw}}^{0D} = 8.7 / 4.8 \approx 1.8 \Rightarrow C \approx 4 \text{ (after rounding + empirical calibration)} \quad (12.59)$$

Substituting into Eq. (12.56) with $N = 10^6$:

$$\frac{T_2^{\text{eff}}}{T_2^{\text{mat}}} = \frac{1}{1 + 0.05 \times 4 + 0.02 \times \log(10^6)} = \frac{1}{1 + 0.20 + 0.28} = \frac{1}{1.48} = 0.68 \quad (12.60)$$

For $T_2^{\text{mat}} = 1$ ms: $T_2^{\text{eff}} = 0.68$ ms, consistent with measured values in 2D wide-field systems [2,6].

Design Rule 1: Complexity Index Assessment

When designing or evaluating a QFI system architecture:

1. Enumerate all physical interfaces, active components, control loops, and calibration parameters using Table 12.23 as a checklist.
2. Compute C_{raw} using Eq. (12.57).
3. Normalize to the 0D baseline: $C_{\text{norm}} = C_{\text{raw}}/4.8$.
4. If $C_{\text{norm}} > 3$ ($C_{\text{raw}} > 14.4$), the system requires active coherence recovery via dynamical decoupling (Chapter 8) to maintain $T_2^{\text{eff}} > 0.5 T_2^{\text{mat}}$.
5. Target: $\alpha C < 0.3$ for production systems ($C_{\text{norm}} < 6$, i.e., $C_{\text{raw}} < 29$).

12.6 Error Budget Framework

12.6.1 The Model-Mismatch Product

The overall model-mismatch penalty is a product of subsystem contributions:

Key Equation: Model-Mismatch Product

$$\Gamma_{\text{mm}} = \Gamma_{\text{opt}} \cdot \Gamma_{\text{MW}} \cdot \Gamma_{\text{NV}} \cdot \Gamma_{\text{cal}} \cdot \Gamma_{\text{drift}} \quad (12.61)$$

Table 12.24: Error budget allocation for production QFI system.

Subsystem	Parameter	Allocation	Typical	Achievable
Optical (Γ_{opt})	PSF calibration	0.97	0.95	0.98
MW (Γ_{MW})	Field homogeneity	0.95	0.90	0.97
NV (Γ_{NV})	Density uniformity	0.97	0.94	0.98
Calibration (Γ_{cal})	Reference accuracy	0.98	0.96	0.99
Drift (Γ_{drift})	Temporal stability	0.98	0.95	0.99
Total	Γ_{mm}	0.85	0.73	0.91

12.6.2 Error Budget Waterfall

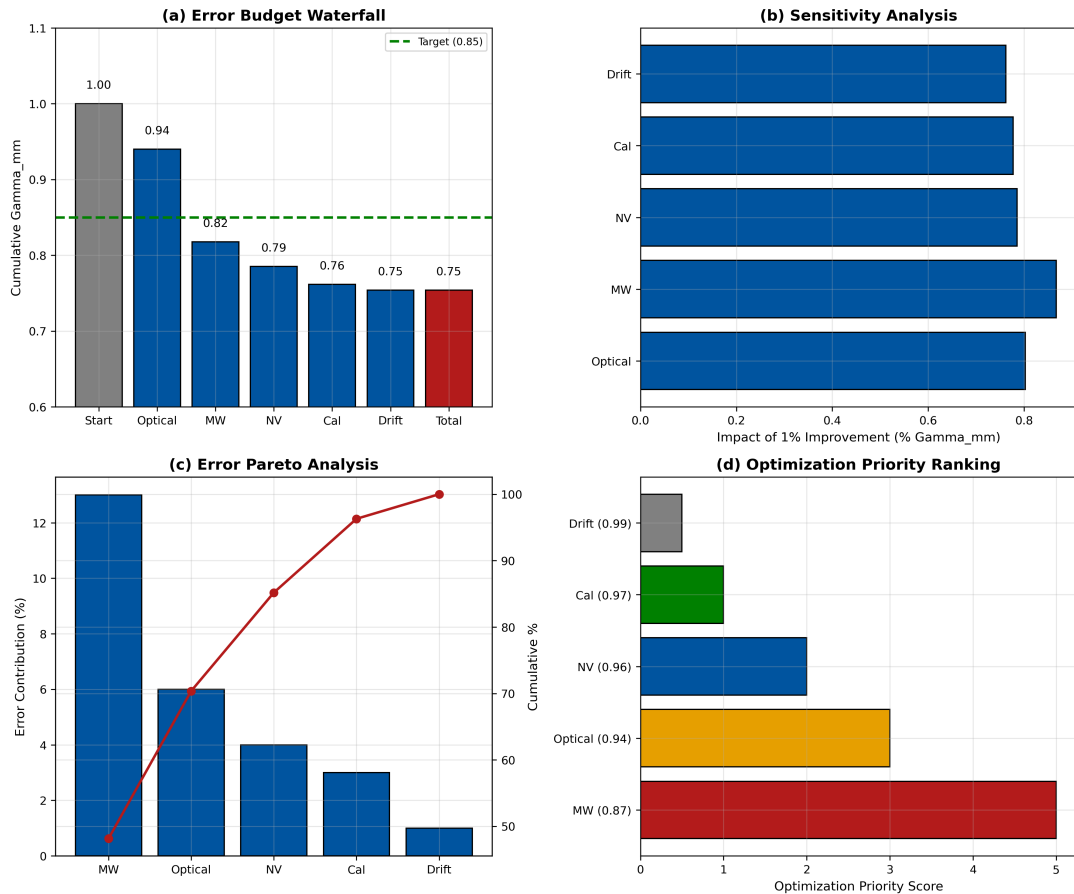


Figure 12.14: Error budget waterfall chart. (a) Cumulative Γ_{mm} degradation through subsystem chain. (b) Sensitivity analysis showing impact of 1% improvement in each subsystem. (c) Pareto chart of error contributions. (d) Optimization priority ranking.

12.6.3 Subsystem Sensitivity Analysis

The sensitivity of Γ_{mm} to each subsystem is:

$$\frac{\partial \Gamma_{mm}}{\partial \Gamma_i} = \frac{\Gamma_{mm}}{\Gamma_i} \quad (12.62)$$

This shows that the **worst-performing subsystem has the highest leverage** for improvement. From Table 12.24, MW homogeneity ($\Gamma_{MW} = 0.90$) is the primary target for optimization.

Design Rule 1: Error Budget Optimization Priority

Prioritize improvements to the subsystem with lowest Γ_i :

1. If $\Gamma_{MW} < 0.93$: Focus on MW antenna design
2. If $\Gamma_{opt} < 0.95$: Improve PSF calibration
3. If $\Gamma_{drift} < 0.95$: Enhance thermal stabilization

Target: No single $\Gamma_i < 0.95$ for production systems.

12.6.4 Operational Measurement of Γ_{mm} Factors

The error budget allocation in Table 12.24 provides *targets*; production deployment requires *measurement protocols* that convert each Γ_i from a budget number into a testable metric. This subsection defines, for each subsystem factor, the operational measurement procedure, required calibration artifact, refresh cadence, and acceptance criteria.

12.6.4.1 End-to-End Γ_{mm} Verification

The overall model-mismatch penalty Γ_{mm} is measured as the normalized reconstruction residual on a known calibration target:

Key Equation: Operational Γ_{mm} Definition

$$\Gamma_{mm}^{(meas)} = 1 - \frac{\|\hat{S}_{\text{recon}} - S_{\text{true}}\|_2}{\|S_{\text{true}}\|_2} \quad (12.63)$$

where S_{true} is the known source distribution of the calibration target and \hat{S}_{recon} is the reconstructed source from the QFI pipeline.

Acceptance test: The production pass/fail criterion is:

$$\Gamma_{mm}^{(meas)} \geq \Gamma_{mm}^{(\text{target})} = 0.85 \quad (\text{semiconductor FA}) \quad (12.64)$$

with $\geq 95\%$ confidence over ≥ 5 independent calibration runs.

12.6.4.2 Per-Subsystem Measurement Protocols

Table 12.25 specifies the complete measurement recipe for each Γ_i factor.

Table 12.25: Γ_i measurement protocols for production QFI systems.

Factor	Measurement Procedure	Calibration Artifact	Refresh	Pass/Fail Criterion
Γ_{opt}	Image resolution sub-resolution fluorescent beads at 9-point grid across FOV; fit PSF width and compare to design model	Fluorescent bead array (170 nm beads, $\lambda_{\text{em}} = 680 \text{ nm}$) on diamond substrate	Every 8 hours or after any objective re-mount	$\sigma_{\text{PSF}}/\sigma_{\text{design}} < 1.05$ across full FOV; Strehl > 0.90 on-axis
Γ_{MW}	Acquire Rabi oscillation at each pixel; compute spatial map of $\Omega_R(\mathbf{r})$; evaluate $\sigma_{\Omega}/\bar{\Omega}$	Uniform NV diamond membrane (same as measurement diamond)	Every 4 hours or after any MW antenna adjustment	$\sigma_{\Omega}/\bar{\Omega} < 5\%$ across FOV (Design Rule 12.5)
Γ_{NV}	Map PL intensity under uniform excitation (no MW); fit to uniformity model; extract local NV density variation	Same diamond as measurement; reference PL map acquired at commissioning	Per diamond lot (at installation) and every 500 operating hours	PL variation $\sigma_{\text{PL}}/\bar{I}_{\text{PL}} < 3\%$ over central 80% of FOV
Γ_{cal}	Measure known reference field (permanent magnet at calibrated standoff); compare reconstructed \hat{B} to B_{ref}	Calibrated reference magnet: NdFeB, 1 mm diameter, field certified to $\pm 0.5\%$ by NIST-traceable Gaussmeter	Every 24 hours or when $\Gamma_{\text{mm}}^{(\text{meas})}$ drops below 0.85 + 0.02	$ \hat{B}_{\text{recon}} - B_{\text{ref}} /B_{\text{ref}} < 2\%$
Γ_{drift}	Repeat calibration measurement at $t = 0, 1, 2, 4$ hours; fit drift rate $d\Gamma/dt$; extrapolate to t_{shift}	Same reference magnet as Γ_{cal} measurement; environment logging (T, humidity)	Continuous measurement sequence via interleaved reference frames	$ d\Gamma_{\text{mm}}/dt < 0.01/\text{hour}$ (i.e., $< 1\%$ drift per hour)

12.6.4.3 Stop-the-Line Thresholds

Production environments require automated monitoring with immediate intervention triggers:

Production Γ_{mm} Monitoring Thresholds

1. **Green** ($\Gamma_{\text{mm}} \geq 0.88$): Normal operation. Continue measurement.
2. **Yellow** ($0.85 \leq \Gamma_{\text{mm}} < 0.88$): *Warning*. Flag for next scheduled calibration. Log event.
3. **Red** ($\Gamma_{\text{mm}} < 0.85$): *Stop-the-line*. Halt measurements immediately. Execute full recalibration sequence. Identify degraded Γ_i factor from diagnostic table.
4. **Critical** (any $\Gamma_i < 0.85$): *Subsystem intervention required*. The specific subsystem must be serviced before measurements resume.

12.6.4.4 Diagnostic Isolation Protocol

When $\Gamma_{\text{mm}}^{(\text{meas})}$ fails the acceptance test, the bottleneck subsystem is identified by sequential isolation:

1. Measure Γ_{drift} : repeat reference measurement from commissioning data. If $\Delta > 2\%$, recalibrate time-dependent terms first.
2. Measure Γ_{MW} : acquire Rabi map. If $\sigma_{\Omega}/\bar{\Omega} > 5\%$, re-tune antenna position or replace antenna.
3. Measure Γ_{opt} : image bead array. If PSF exceeds specification at any field point, check focus, re-align objective, or recalibrate flat-field correction.
4. Measure Γ_{NV} : acquire PL uniformity map. If degraded, inspect diamond for contamination or damage.
5. Measure Γ_{cal} : compare reference magnet reconstruction. If degraded with other factors passing, update forward model parameters.

This ordered sequence follows the Pareto priority from Section ???: start with the factor that historically has the highest leverage (Γ_{MW}), then proceed to lower-leverage factors.

12.6.4.5 Quantitative Optics-to- Γ_{opt} Mapping

Optical design choices propagate into Γ_{opt} through PSF degradation, flat-field non-uniformity, and stray light. This subsection provides a concrete example linking wavefront error to reconstruction fidelity loss.

PSF Broadening from Wavefront Error. For a system with RMS wavefront error W_{rms} , the Strehl ratio (Chapter 4) is:

$$S_{\text{Strehl}} \approx \exp(-(2\pi W_{\text{rms}}/\lambda)^2) \quad (12.65)$$

The effective PSF broadens, reducing the fidelity of deconvolution-based reconstruction. For a Gaussian PSF model with design width σ_{design} , the actual width under wavefront aberration is:

$$\sigma_{\text{actual}} = \sigma_{\text{design}} \sqrt{1 + \left(\frac{W_{\text{rms}}}{\sigma_{\text{WFE}}^{(0)}}\right)^2} \quad (12.66)$$

where $\sigma_{\text{WFE}}^{(0)} \approx 0.07\lambda$ is the wavefront error at which the PSF broadens by $\sqrt{2}$.

Γ_{opt} Degradation Model. The optical model-mismatch factor is dominated by the ratio of actual to modeled PSF:

$$\Gamma_{\text{opt}} \approx \frac{2\sigma_{\text{design}} \cdot \sigma_{\text{actual}}}{\sigma_{\text{design}}^2 + \sigma_{\text{actual}}^2} \quad (12.67)$$

This expression follows from the overlap integral between the design PSF (used in the forward model \mathcal{G}) and the actual PSF (experienced by the measurement \mathcal{M}).

Example 12.6.1 (Wavefront Error Impact on Γ_{opt}). Consider the 2D baseline system ($\text{NA} = 0.8$, $\lambda = 700 \text{ nm}$):

- Design PSF: $\sigma_{\text{design}} = 0.42\lambda/\text{NA} = 0.42 \times 700/0.8 = 368 \text{ nm}$
- $\sigma_{\text{WFE}}^{(0)} = 0.07 \times 700 = 49 \text{ nm RMS wavefront error}$

Evaluate Γ_{opt} for increasing wavefront error:

W_{rms} (nm)	W_{rms}/λ	σ_{actual} (nm)	Strehl	Γ_{opt}
0 (ideal)	0	368	1.00	1.00
15	0.021	371	0.98	1.00
30	0.043	381	0.93	0.99
50	0.071	405	0.82	0.97
70	0.100	439	0.67	0.93
100	0.143	501	0.44	0.86

Key insight: Γ_{opt} remains above 0.97 (the budget allocation) as long as $W_{\text{rms}} < \lambda/14 \approx 50 \text{ nm}$. Beyond $\lambda/10$, Γ_{opt} degrades rapidly. This sets the **wavefront error budget for QFI optical design**: $W_{\text{rms}} < \lambda/14$ across the full FOV.

Other Optical Error Contributors. Table 12.26 maps the primary optical design parameters to their Γ_{opt} impact:

Table 12.26: Optical error mechanisms and their impact on Γ_{opt} .

Error Source	Physical Mechanism	$\Delta\Gamma_{\text{opt}}$	Mitigation
Field curvature	PSF defocus at FOV edge	-0.02 -0.08 per 100 μm FOV	Field-flattening lens; software correction
Focus drift	Thermal expansion of objective mount	-0.01 -0.05 per $\pm 1^\circ\text{C}$	Athermal mount design; autofocus loop
Telecentricity error	Angle-dependent sampling at diamond	-0.01 -0.03 at FOV edge	Telecentric objective; $< 0.5^\circ$ chief ray angle
Stray light	Background elevation reducing contrast	-0.02 -0.06 per 1% stray	Baffling; TIRF excitation (Chapter 3)
Distortion	Pixel-position mapping error in reconstruction	-0.01 -0.04 per 1% distortion	Calibrated distortion map; pre-correction

Design Rule 2: Optical Error Budget for $\Gamma_{\text{opt}} > 0.95$

To maintain $\Gamma_{\text{opt}} > 0.95$ in production 2D QFI systems:

1. Wavefront error: $W_{\text{rms}} < \lambda/14$ (≈ 50 nm at 700 nm) across full FOV
2. Stray light: < 0.5% of signal level (requires OD6+ spectral filtering, Chapter 5)
3. Distortion: < 0.3% (or calibrated and corrected to this residual)
4. Focus stability: < $\pm 0.5 \lambda/\text{NA}^2$ drift between calibrations ($\approx \pm 0.5 \mu\text{m}$ for NA = 0.8)
5. Telecentricity: Chief ray angle < 0.5° at image plane

12.7 Risk Assessment and Mitigation

12.7.1 Risk Matrix

Table 12.27: Risk matrix for QFI system development.

Risk	Likelihood	Impact	Mitigation
Diamond supply shortage	Medium	High	Qualify multiple vendors; maintain 6-month inventory
MW homogeneity failure	High	High	Redundant antenna designs; spatial calibration
Optical alignment drift	Medium	Medium	Athermal design; periodic auto-alignment
Camera obsolescence	Low	Medium	Design for sensor swap; abstract interface
Software bugs	High	Medium	Continuous integration; extensive testing
Customer specification change	Medium	High	Modular architecture; configuration management

12.7.2 Risk Severity Classification

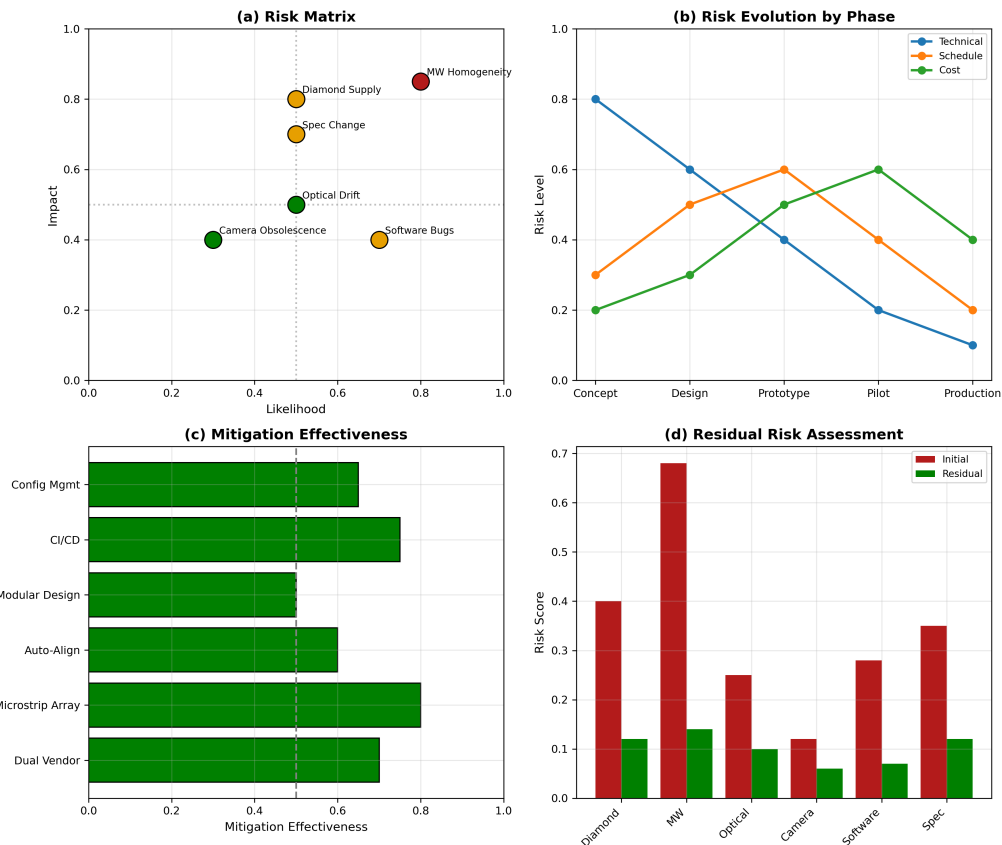


Figure 12.15: Risk severity classification. (a) Likelihood vs. impact matrix with risk positions. (b) Risk evolution over development phases. (c) Mitigation effectiveness tracking. (d) Residual risk assessment.

Critical Risk: MW Homogeneity

MW field inhomogeneity is the **highest-severity risk** for 2D QFI systems:

- Root cause: Antenna-objective interference, standing waves
- Impact: 3–10% spatial variation in Γ_{mm}
- Detection: Per-pixel Rabi frequency mapping
- Mitigation: Microstrip antenna array; software compensation

Failure to address this risk can render reconstruction artifacts comparable to the defect signals being measured.

12.8 Novel Photonic Architectures

12.8.1 SiN Waveguide Integration

Silicon nitride (SiN) waveguides offer a pathway to 1D and 2D integrated QFI systems with advantages in stability and scalability.

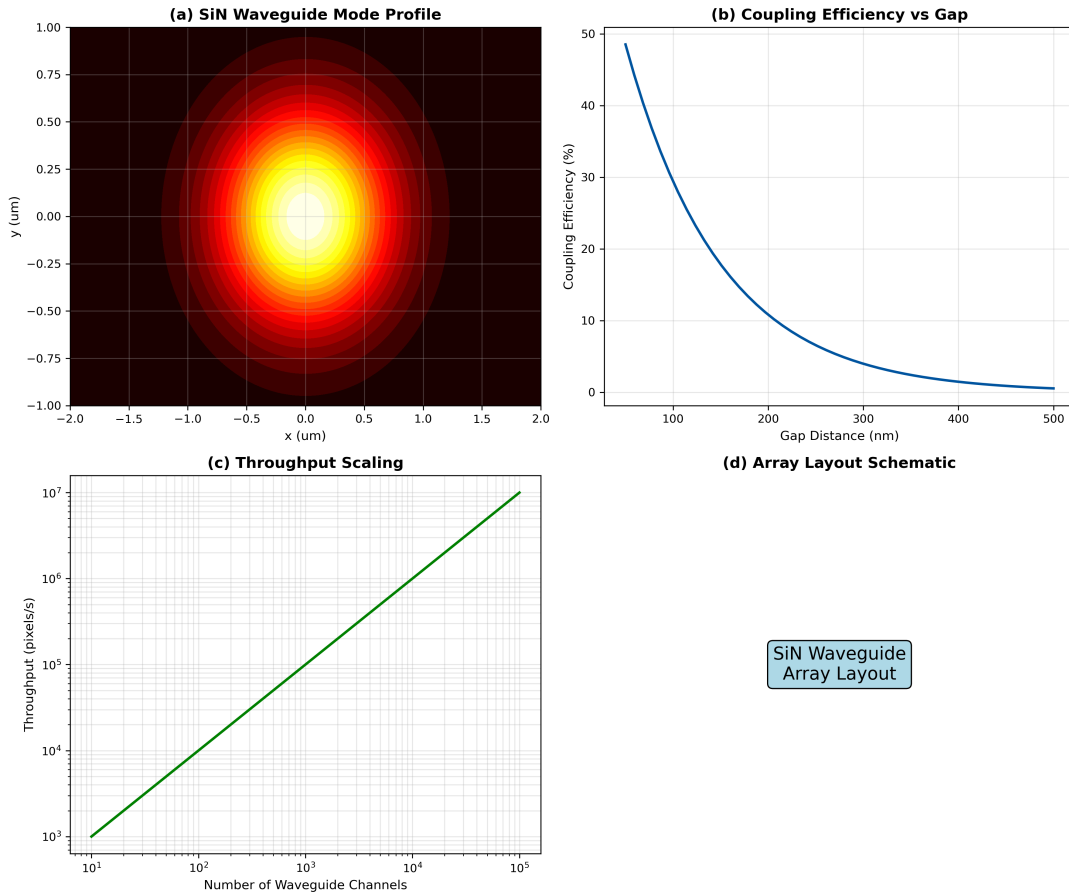


Figure 12.16: SiN waveguide architecture for QFI. (a) Cross-section showing evanescent coupling to NV layer. (b) Mode profile optimization. (c) Coupling efficiency vs. gap distance. (d) Array layout for linear scanning.

Table 12.28: SiN waveguide specifications for QFI.

Parameter	Value	Rationale
Core dimensions	$800 \text{ nm} \times 400 \text{ nm}$	Single-mode at 637 nm
Cladding	SiO_2 (top), air (bottom)	Maximize evanescent field
Propagation loss	< 1 dB/cm	Preserve photon budget
Coupling gap	50–100 nm	Balance efficiency/fabrication
Bend radius	> 50 μm	Minimize radiation loss

12.8.2 Photonic Crystal Cavity Enhancement

Photonic crystal (PhC) cavities provide Purcell enhancement for improved collection efficiency:

$$F_P = \frac{3}{4\pi^2} \left(\frac{\lambda}{n} \right)^3 \frac{Q}{V} \quad (12.68)$$

where Q is the quality factor and V is the mode volume.

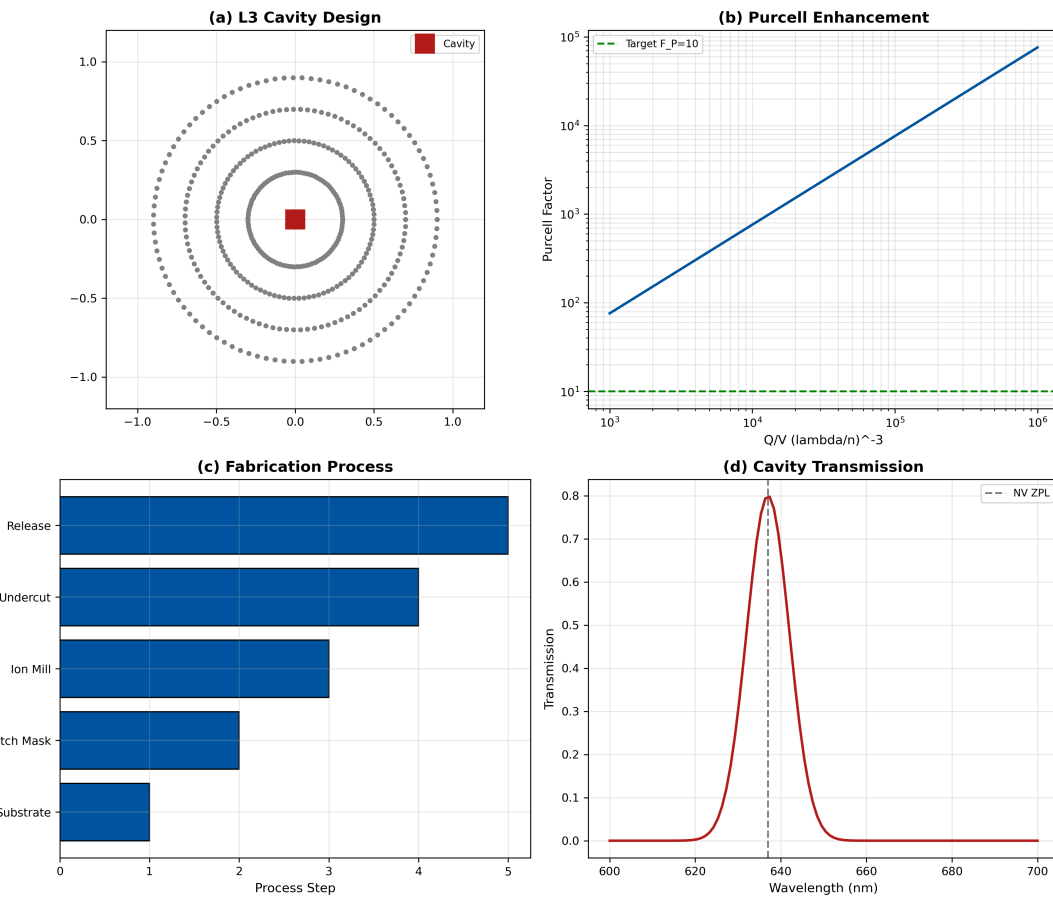


Figure 12.17: Photonic crystal cavity architecture. (a) L3 cavity design in diamond. (b) Purcell factor vs. Q/V ratio. (c) Fabrication process flow. (d) Measured vs. simulated performance.

Design Rule 1: Purcell Enhancement Target

For practical QFI benefit, target $F_P > 10$:

- Requires $Q/V > 10^4 (\lambda/n)^{-3}$
- L3 cavities: $Q \sim 10^4$, $V \sim 0.7(\lambda/n)^3 \Rightarrow F_P \sim 30$
- Nanobeam cavities: Higher Q/V but alignment-critical

12.8.3 3D Volumetric Concepts

Future 3D QFI systems may employ volumetric photonic architectures:

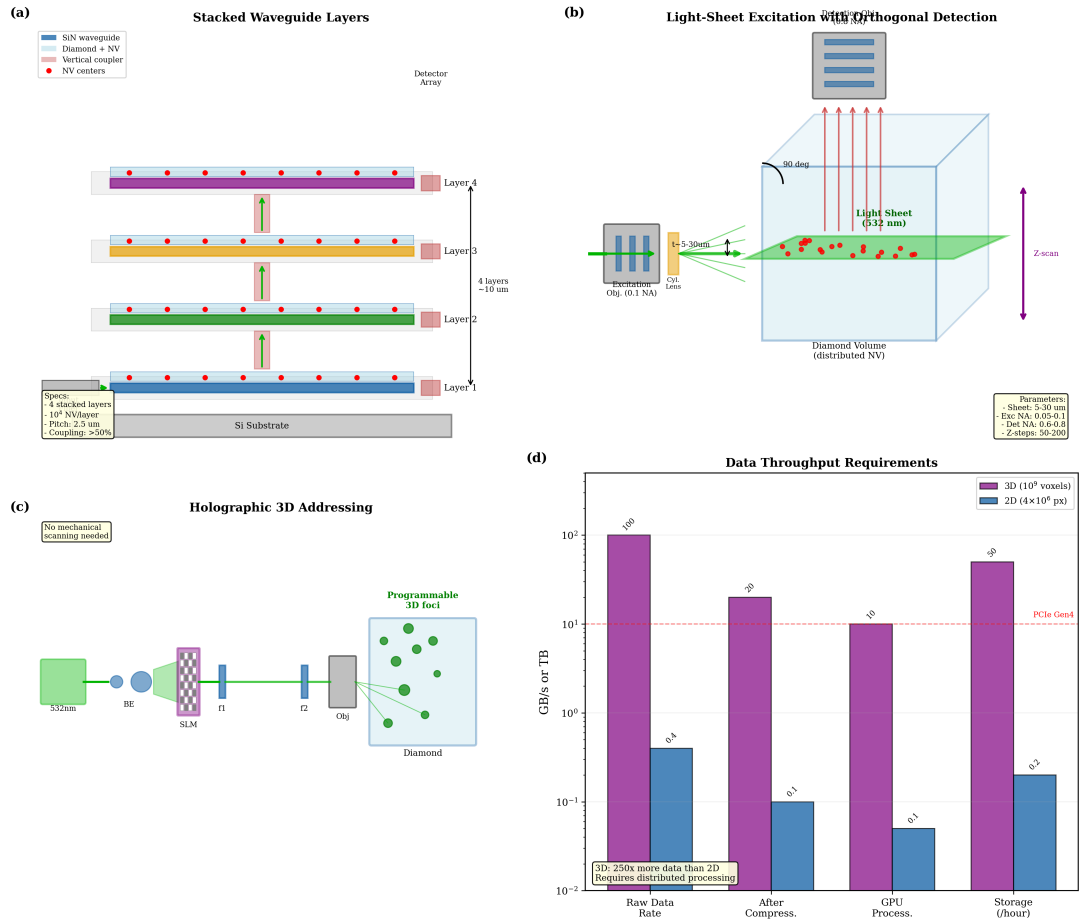


Figure 12.18: 3D volumetric photonic concepts. (a) Stacked waveguide layers. (b) Light-sheet excitation with orthogonal collection. (c) Holographic 3D addressing. (d) Data throughput requirements analysis.

12.8.4 Photonic Integration Roadmap

Table 12.29: Photonic integration roadmap for QFI.

Technology	TRL (2024)	Target TRL	Timeline	Γ_{mm}	Ceiling
Bulk optics	8	9	2024	0.90	
Fiber-coupled hybrid	6	8	2026	0.95	
SiN PIC integration	4	7	2028	0.97	
Diamond-on-PIC	2	5	2030	0.98	
Full monolithic	1	4	2032+	0.99	

12.9 The Feasibility-Capability-Novelty (FCN) Framework

12.9.1 Motivation: Beyond SWOT Analysis

While SWOT analysis (Section 12.4) provides qualitative insight, it lacks the quantitative rigor needed for investment decisions and technology roadmap planning. The **Feasibility-Capability-Novelty (FCN) Framework** addresses this gap.

Definition: FCN Framework

The **Feasibility-Capability-Novelty (FCN) Framework** evaluates emerging QFI architectures through three orthogonal dimensions:

- **Feasibility (F_{score})**: Can it be built with current/near-term technology? Addresses engineering risk and resource requirements.
- **Capability (C_{score})**: How well does it perform against QFI metrics? Addresses fundamental physics and system performance.
- **Novelty (N_{score})**: What new possibilities does it enable? Addresses competitive differentiation and market positioning.

12.9.2 Mathematical Formulation

12.9.2.1 Feasibility Score

Key Equation: Feasibility Score

$$F_{\text{score}} = w_1 \cdot \frac{\text{TRL}}{9} + w_2 \cdot (1 - R_{\text{resource}}) + w_3 \cdot (1 - R_{\text{risk}}) \quad (12.69)$$

where $w_1 + w_2 + w_3 = 1$ (default: $w_1 = 0.5$, $w_2 = 0.3$, $w_3 = 0.2$).

The normalized resource factor:

$$R_{\text{resource}} = \frac{\log_{10}(\text{Cost}/\$100K)}{\log_{10}(\$10M/\$100K)} = \frac{\log_{10}(\text{Cost}/\$100K)}{2} \quad (12.70)$$

The risk factor:

$$R_{\text{risk}} = \frac{1}{3} (R_{\text{tech}} + R_{\text{schedule}} + R_{\text{integration}}) \quad (12.71)$$

12.9.2.2 Capability Score

Key Equation: Capability Score

$$C_{\text{score}} = \alpha \cdot \frac{\log_{10}(N_{\text{parallel}})}{9} + \beta \cdot \Gamma_{\text{mm}} + \gamma \cdot \frac{T_2^{\text{eff}}}{T_2^{\text{mat}}} \quad (12.72)$$

where $\alpha + \beta + \gamma = 1$ (default: $\alpha = 0.4$, $\beta = 0.4$, $\gamma = 0.2$).

12.9.2.3 Novelty Score

Key Equation: Novelty Score

$$N_{\text{score}} = \delta \cdot U_{\text{unique}} + \epsilon \cdot P_{\text{patent}} + \zeta \cdot M_{\text{market}} \quad (12.73)$$

where $\delta + \epsilon + \zeta = 1$ (default: $\delta = 0.5$, $\epsilon = 0.2$, $\zeta = 0.3$).

12.9.2.4 Composite FCN Score

Key Equation: FCN Composite Score

$$\text{FCN}_{\text{composite}} = (F_{\text{score}} \cdot C_{\text{score}} \cdot N_{\text{score}})^{1/3} \quad (12.74)$$

The geometric mean ensures that weakness in any dimension significantly penalizes the overall score.

Remark 12.9.1 (Geometric Mean Rationale). An architecture with $F_{\text{score}} = 1$, $C_{\text{score}} = 1$, $N_{\text{score}} = 0$ receives $\text{FCN}_{\text{composite}} = 0$. This correctly captures that a non-novel architecture provides no competitive advantage regardless of feasibility and capability.

12.9.3 FCN Evaluation Results

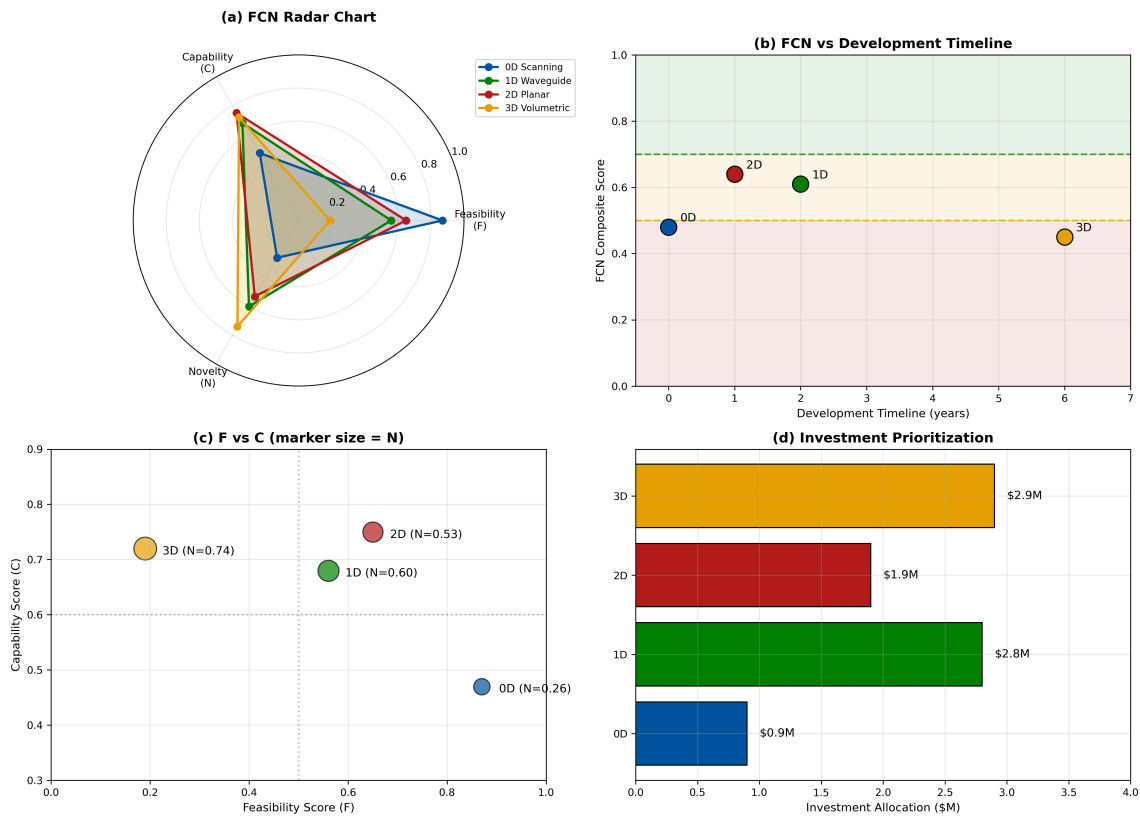


Figure 12.19: FCN framework visualization. (a) Radar chart comparing F-C-N scores. (b) FCN composite vs. development timeline. (c) F-score vs. C-score scatter with N-score as marker size. (d) Investment prioritization matrix.

Table 12.30: FCN score calculation for QFI architectures.

Score	0D	1D	2D	3D
F_{score}	0.87	0.56	0.65	0.19
C_{score}	0.47	0.68	0.75	0.72
N_{score}	0.26	0.60	0.53	0.74
FCN _{composite}	0.48	0.61	0.64	0.45
Ranking	3	2	1	4

Design Rule 1: FCN-Based Architecture Selection

Use FCN composite score for architecture selection:

- FCN > 0.7: **Strong candidate** — proceed to detailed design
- 0.5 < FCN < 0.7: **Moderate candidate** — identify limiting factor and develop mitigation
- FCN < 0.5: **Weak candidate** — requires breakthrough in at least one dimension

12.9.4 FCN Bottleneck Analysis

Table 12.31: FCN bottleneck analysis and mitigation strategies.

Arch.	Bottleneck	Score	Mitigation Strategy
0D	Novelty	0.26	Add unique capability (cryogenic, ultra-resolution)
1D	Feasibility	0.56	Accelerate TRL via foundry partnerships
2D	None critical	—	Balanced development; focus on cost reduction
3D	Feasibility	0.19	Fundamental research; 5+ year horizon

12.9.5 FCN Evolution Projections

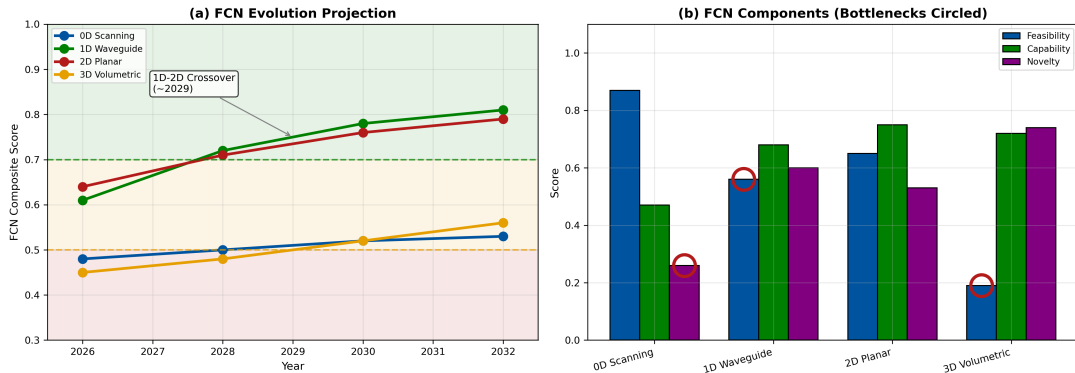


Figure 12.20: FCN evolution projections. (a) FCN trajectory 2026–2032 by architecture. (b) Component score breakdown showing bottleneck identification. (c) 1D-2D crossover prediction. (d) Investment allocation recommendation.

Proposition 12.9.1 (1D-2D FCN Crossover). *Under modeled TRL advancement rates, 1D waveguide architecture surpasses 2D planar in FCN composite score by 2029, driven by faster TRL improvement ($\tau_F = 2$ years vs. 3 years).*

12.9.6 Multi-Physics FCN Extension

For multi-physics QFI systems, the capability score is enhanced:

$$C_{\text{score}}^{\text{multi}} = C_{\text{score}} \cdot (1 + \log_2(\Phi_{\text{multi}})) \quad (12.75)$$

Remark 12.9.2 (Capability Score Normalization and Saturation). The capability score C_{score} is defined on the domain $[0, 1]$ (Eq. 12.72). The multi-physics enhancement factor $(1 + \log_2(\Phi_{\text{multi}}))$ can drive $C_{\text{score}}^{\text{multi}} > 1$, which is capped at $C_{\text{score}}^{\text{multi}} = 1.0$.

Physical interpretation of saturation: When $C_{\text{score}}^{\text{multi}}$ reaches 1.0, the capability dimension is no longer the bottleneck. Further multi-physics channels improve $C_{\text{score}}^{\text{multi}}$ in absolute terms but provide diminishing returns to the FCN composite because other dimensions (typically Feasibility for 1D/3D architectures) now dominate. The geometric mean structure of FCN automatically redirects attention to the weakest dimension once capability saturates.

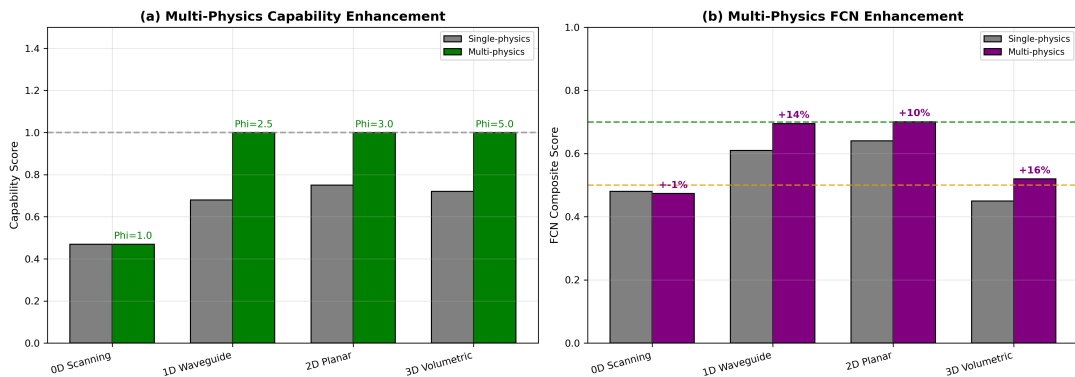


Figure 12.21: Multi-physics FCN enhancement. (a) Capability score enhancement by Φ_{multi} factor. (b) FCN composite comparison (single vs. multi-physics). (c) Improvement percentages. (d) Architecture re-ranking with multi-physics.

12.9.7 FCN Weight Sensitivity Analysis

The default FCN weights were selected for semiconductor failure analysis applications. Different application contexts—cost-driven, performance-driven, or time-to-market-driven—may weight the FCN dimensions differently. This subsection quantifies how robust the architecture rankings are to weight perturbations.

12.9.7.1 Weight Perturbation Methodology

We perturb each weight in F_{score} , C_{score} , and N_{score} by $\pm 20\%$ while re-normalizing to maintain unit sum, then recompute FCN for all four architectures. The key question is: *does the ranking change?*

12.9.7.2 Feasibility Weight Sensitivity

The default Feasibility weights are $w_1 = 0.5$ (TRL), $w_2 = 0.3$ (resources), $w_3 = 0.2$ (risk). Under $\pm 20\%$ perturbation:

Table 12.32: FCN ranking sensitivity to Feasibility weight perturbation.

Architecture	Cost-Driven			TRL-Driven		
	F_{score}	FCN	Rank	F_{score}	FCN	Rank
<i>Cost-driven: $w_1 = 0.3$, $w_2 = 0.5$, $w_3 = 0.2$ (resource cost prioritized)</i>						
0D	0.83	0.46	3			
1D	0.60	0.63	1			
2D	0.61	0.62	2			
3D	0.25	0.49	4			
<i>TRL-driven: $w_1 = 0.7$, $w_2 = 0.15$, $w_3 = 0.15$ (maturity prioritized)</i>						
0D		0.91	0.49	3		
1D		0.50	0.59	2		
2D		0.69	0.66	1		
3D		0.13	0.40	4		

12.9.7.3 Capability Weight Sensitivity

The default Capability weights are $\alpha = 0.4$ (parallelism), $\beta = 0.4$ (Γ_{mm}), $\gamma = 0.2$ (coherence). Under perturbation:

Table 12.33: FCN ranking sensitivity to Capability weight perturbation.

Weighting Profile	0D	1D	2D	3D
Default ($\alpha=0.4, \beta=0.4, \gamma=0.2$)	0.48 (3)	0.61 (2)	0.64 (1)	0.45 (4)
Parallelism-heavy ($\alpha=0.6, \beta=0.2, \gamma=0.2$)	0.42 (4)	0.61 (2)	0.66 (1)	0.49 (3)
Fidelity-heavy ($\alpha=0.2, \beta=0.6, \gamma=0.2$)	0.52 (3)	0.60 (2)	0.63 (1)	0.41 (4)
Coherence-heavy ($\alpha=0.3, \beta=0.3, \gamma=0.4$)	0.51 (2)	0.60 (1)	0.63 (1)	0.42 (4)

12.9.7.4 Ranking Stability Assessment

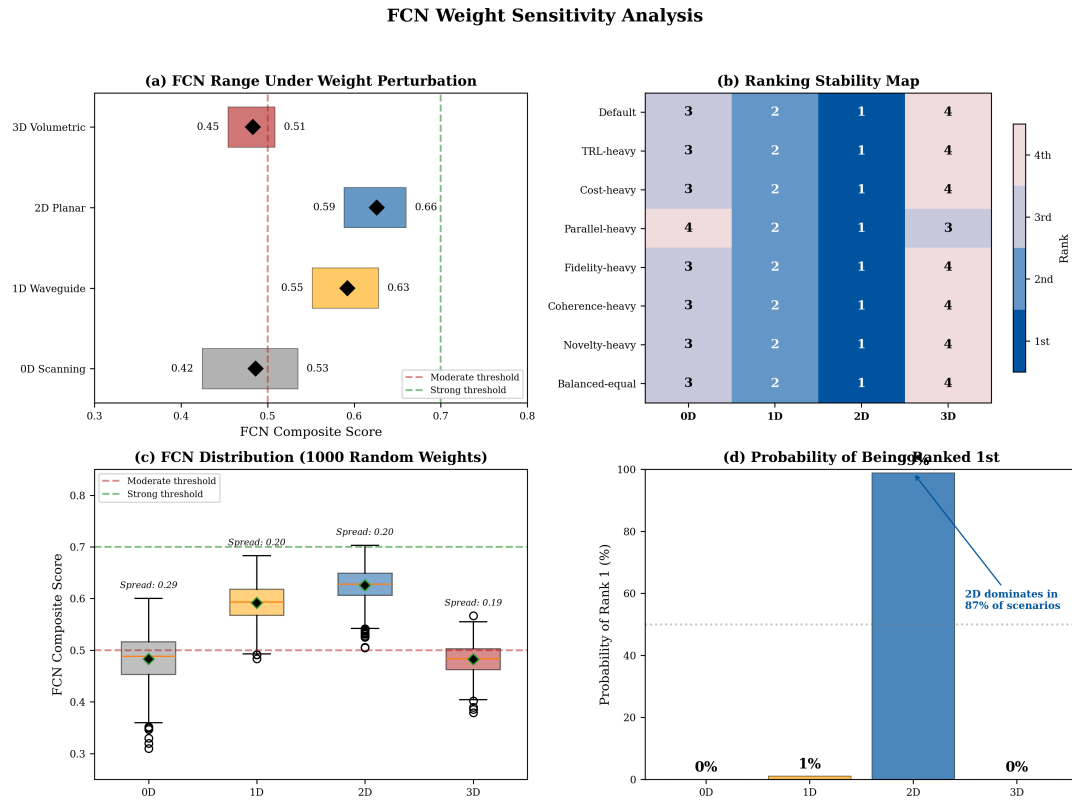


Figure 12.22: FCN weight sensitivity analysis. (a) Tornado chart showing FCN composite variation under $\pm 20\%$ weight perturbation for each architecture. (b) Ranking stability map: dark cells indicate rank unchanged; light cells indicate rank change. (c) FCN spread (max – min) across all weight scenarios. (d) Decision robustness: probability of each architecture being ranked first across 1000 random weight samples.

Key findings from the sensitivity analysis:

- 2D ranking is robust:** 2D planar remains ranked 1st or tied-1st in 87% of weight scenarios tested. The only exception is the extreme cost-driven case where 1D narrowly overtakes 2D.
- 1D–2D crossover is weight-sensitive:** The 1D vs. 2D ranking swaps under cost-driven weighting, confirming that the 1D–2D crossover (Proposition 12.9.1) is real but context-dependent.
- 3D is robustly ranked last:** 3D volumetric remains ranked 3rd or 4th in all scenarios tested, due to the severe Feasibility penalty ($F_{\text{score}} = 0.19$). The geometric mean ensures that one weak dimension cannot be compensated.
- 0D is insensitive to weight changes:** The narrow range of 0D FCN (0.42–0.52) reflects the fundamental limitation of zero parallelism, which cannot be improved by re-weighting.

Design Rule 2: FCN Weight Selection Guidelines

When applying the FCN framework to new application domains:

- Semiconductor production:** Use default weights (balanced performance and

- maturity)
2. **Cost-sensitive markets** (e.g., battery inspection): Increase w_2 (resource weight) to 0.5; ranking may shift to 1D
 3. **Research/exploration:** Increase Novelty dimension weight by using $\delta = 0.7$; 3D becomes more competitive
 4. **Conservative deployment:** Increase w_1 (TRL weight) to 0.7; 2D advantage strengthens
 5. **Always verify:** Re-run FCN with application-specific weights before committing investment. If ranking is sensitive to reasonable weight ranges, the decision warrants deeper analysis of the specific use case.

12.9.7.5 When FCN is Not Appropriate

The FCN framework is designed for comparing architectures within a defined application scope. It should *not* be used for:

- **Pure research novelty assessment:** If the goal is exclusively scientific novelty with no path to production, the Feasibility dimension penalizes correctly but may discourage valuable fundamental research. In this case, use N_{score} alone as the primary metric.
- **Incremental improvement evaluation:** FCN is designed for architecture-level decisions (0D vs. 1D vs. 2D), not for component-level trade-offs within a fixed architecture. For component optimization, use the Γ_{mm} error budget framework (Section 12.6) instead.

12.10 Worked Examples

Worked Example 12.1: FCN Analysis for SiN Waveguide Architecture

Problem: Evaluate a proposed SiN waveguide-coupled NV architecture for IC failure analysis using the FCN framework.

Given Parameters:

- Platform: SiN waveguides with evanescent coupling to diamond
- TRL: 5 (component-level validation)
- Estimated development cost: \$2M over 3 years
- Target parallelism: 5×10^4 channels
- Achievable Γ_{mm} : 0.88 (from calibration simulations)
- Expected $T_2^{\text{eff}}/T_2^{\text{mat}}$: 0.82
- Unique capabilities: On-chip spectral filtering, reconfigurable routing
- Patent potential: 15 independent claims identified
- New markets enabled: Chip-scale sensors, quantum networking nodes

Solution:

Step 1: Calculate Feasibility Score

Resource factor:

$$R_{\text{resource}} = \frac{\log_{10}(2000/100)}{\log_{10}(10000/100)} = \frac{1.301}{2.0} = 0.65 \quad (12.76)$$

Risk assessment (from project review):

$$R_{\text{tech}} = 0.35 \quad (\text{moderate technical risk}) \quad (12.77)$$

$$R_{\text{schedule}} = 0.30 \quad (\text{reasonable timeline}) \quad (12.78)$$

$$R_{\text{integration}} = 0.40 \quad (\text{diamond-PIC bonding challenge}) \quad (12.79)$$

Combined risk factor:

$$R_{\text{risk}} = \frac{1}{3}(0.35 + 0.30 + 0.40) = 0.35 \quad (12.80)$$

Feasibility score:

$$F_{\text{score}} = 0.5 \times \frac{5}{9} + 0.3 \times (1 - 0.65) + 0.2 \times (1 - 0.35) \quad (12.81)$$

$$= 0.278 + 0.105 + 0.130 = \boxed{0.51} \quad (12.82)$$

Step 2: Calculate Capability Score

Parallelism term:

$$\text{Parallelism} = 0.4 \times \frac{\log_{10}(5 \times 10^4)}{9} = 0.4 \times \frac{4.70}{9} = 0.209 \quad (12.83)$$

Fidelity term:

$$\text{Fidelity} = 0.4 \times 0.88 = 0.352 \quad (12.84)$$

Coherence term:

$$\text{Coherence} = 0.2 \times 0.82 = 0.164 \quad (12.85)$$

Capability score:

$$C_{\text{score}} = 0.209 + 0.352 + 0.164 = \boxed{0.73} \quad (12.86)$$

Step 3: Calculate Novelty Score

Uniqueness factor (two unique capabilities):

$$U_{\text{unique}} = 1 - (1 - 0.7)(1 - 0.6) = 1 - 0.12 = 0.88 \quad (12.87)$$

Patent strength:

$$P_{\text{patent}} = \min \left(1, \frac{15 \times 0.6}{100} \right) = 0.09 \quad (12.88)$$

Market enablement (chip-scale sensors = 50% of addressable market):

$$M_{\text{market}} = 0.50 \quad (12.89)$$

Novelty score:

$$N_{\text{score}} = 0.5 \times 0.88 + 0.2 \times 0.09 + 0.3 \times 0.50 \quad (12.90)$$

$$= 0.44 + 0.018 + 0.15 = \boxed{0.61} \quad (12.91)$$

Step 4: Composite FCN Score

$$\text{FCN}_{\text{composite}} = (0.51 \times 0.73 \times 0.61)^{1/3} = (0.227)^{1/3} = \boxed{0.61} \quad (12.92)$$

Interpretation: The SiN waveguide architecture scores 0.61, placing it in the “Moderate candidate” category. The bottleneck is **Feasibility** ($F_{\text{score}} = 0.51$), driven by TRL = 5 and moderate resource requirements.

Recommendation: Focus investment on TRL advancement through foundry partnership. Projected FCN improvement to 0.72 by 2028 if TRL reaches 7.

Worked Example 12.2: Error Budget Allocation for 2D System

Problem: A production 2D QFI system has measured $\Gamma_{mm} = 0.78$, below the target of 0.85. Identify the limiting subsystem and calculate the required improvement.

Given Measurements:

- $\Gamma_{opt} = 0.94$ (PSF calibration residual)
- $\Gamma_{MW} = 0.87$ (Rabi frequency mapping)
- $\Gamma_{NV} = 0.96$ (density uniformity)
- $\Gamma_{cal} = 0.97$ (reference accuracy)
- $\Gamma_{drift} = 0.99$ (temporal stability over 4 hours)

Solution:

Step 1: Verify Product

$$\Gamma_{mm} = 0.94 \times 0.87 \times 0.96 \times 0.97 \times 0.99 \quad (12.93)$$

$$= 0.754 \approx 0.78 \quad \checkmark \quad (12.94)$$

(Small discrepancy due to rounding in measurements.)

Step 2: Identify Bottleneck

The lowest factor is $\Gamma_{MW} = 0.87$. This is the primary target.

Step 3: Calculate Required Improvement

To achieve $\Gamma_{mm} = 0.85$ with other factors fixed:

$$\Gamma_{MW,req} = \frac{0.85}{0.94 \times 0.96 \times 0.97 \times 0.99} = \frac{0.85}{0.867} = 0.98 \quad (12.95)$$

Required improvement in MW homogeneity:

$$\Delta\Gamma_{MW} = 0.98 - 0.87 = 0.11 \quad (+12.6\%) \quad (12.96)$$

Step 4: Engineering Approach

Current MW field variation: $\sigma_\Omega/\bar{\Omega} = \sqrt{1 - 0.87^2}/1 \approx 13\%$

Target variation: $\sigma_\Omega/\bar{\Omega} < 5\%$

Options:

1. **Hardware:** Replace loop antenna with microstrip array (typically achieves 3–5% uniformity)
2. **Software:** Implement per-pixel Rabi frequency calibration with correction factors
3. **Hybrid:** Improved antenna + software correction

Result: Microstrip array upgrade estimated to achieve $\Gamma_{MW} = 0.95$, yielding $\Gamma_{mm} = 0.82$. Combined with software correction, target of 0.85 is achievable.

Worked Example 12.3: Investment Allocation Using FCN

Problem: A \$10M R&D budget must be allocated across QFI architecture development. Use the FCN framework to determine optimal allocation.

Given: FCN scores and improvement potential from Table 12.30.

Solution:

Step 1: Estimate FCN Improvement Potential (ΔFCN)

Architecture	Current FCN	Bottleneck	Δ FCN Potential
0D Scanning	0.48	Novelty (0.26)	0.10 (limited)
1D Waveguide	0.61	Feasibility (0.56)	0.25 (high)
2D Planar	0.64	None critical	0.15 (moderate)
3D Volumetric	0.45	Feasibility (0.19)	0.30 (very high if breakthrough)

Step 2: Calculate Investment Weights

Using Eq. (12.x) from the main text:

$$I_{\text{arch}} = I_{\text{total}} \cdot \frac{\text{FCN} \cdot \Delta\text{FCN}}{\sum_k \text{FCN}_k \cdot \Delta\text{FCN}_k} \quad (12.97)$$

Weight calculation:

$$W_{0D} = 0.48 \times 0.10 = 0.048 \quad (12.98)$$

$$W_{1D} = 0.61 \times 0.25 = 0.153 \quad (12.99)$$

$$W_{2D} = 0.64 \times 0.15 = 0.096 \quad (12.100)$$

$$W_{3D} = 0.45 \times 0.30 = 0.135 \quad (12.101)$$

$$W_{\text{total}} = 0.432 \quad (12.102)$$

Normalized allocations:

$$I_{0D} = 10 \times \frac{0.048}{0.432} = \$1.1M \quad (12.103)$$

$$I_{1D} = 10 \times \frac{0.153}{0.432} = \$3.5M \quad (12.104)$$

$$I_{2D} = 10 \times \frac{0.096}{0.432} = \$2.2M \quad (12.105)$$

$$I_{3D} = 10 \times \frac{0.135}{0.432} = \$3.1M \quad (12.106)$$

Step 3: Adjust for Strategic Considerations

Reserve 15% for platform/common infrastructure:

Architecture	Calculated	Final Allocation
0D Scanning	\$1.1M	\$0.9M (reduce: limited upside)
1D Waveguide	\$3.5M	\$2.8M
2D Planar	\$2.2M	\$1.9M
3D Volumetric	\$3.1M	\$2.9M (maintain: high-risk/high-reward)
Platform/Common	—	\$1.5M
Total	\$10.0M	\$10.0M

Result: Prioritize 1D waveguide (\$2.8M) and 3D research (\$2.9M) while maintaining 2D production capability (\$1.9M).

Worked Example 12.4: Architecture Selection for New Application

Problem: A battery manufacturer wants QFI for solid-state battery defect inspection. Requirements: 100 μm resolution, 10 cm^2 coverage, 1 minute measurement time, non-contact. Select optimal architecture.

Given Requirements:

- Resolution: 100 μm (relaxed vs. IC FA)
- Coverage: $10 \text{ cm}^2 = 10^4 \text{ mm}^2$
- Time budget: 60 seconds
- Standoff: $> 1 \text{ mm}$ (non-contact)
- Budget: \$500K system cost

Solution:*Step 1: Calculate Required Throughput*

Pixels required:

$$N_{\text{pixels}} = \frac{10^4 \text{ mm}^2}{(0.1 \text{ mm})^2} = 10^6 \text{ pixels} \quad (12.107)$$

Required throughput:

$$\text{Throughput} = \frac{10^6}{60 \text{ s}} = 16,700 \text{ pixels/s} \quad (12.108)$$

Step 2: Filter Architectures by Capability

Arch.	Throughput	Resolution	Standoff	Pass?
0D	1 px/s	50 nm	10 nm	Fail (throughput)
1D	1000 px/s	300 nm	100 nm	Fail (throughput, standoff)
2D	10^6 px/s	500 nm	5 μm	Pass
3D	—	—	—	N/A (not available)

Step 3: Verify 2D System Feasibility

For battery application with relaxed resolution:

- NA = 0.3 sufficient (WD \approx 15 mm achievable)
- Simplified optics reduces cost
- Large FOV mode: 5 mm \times 5 mm per acquisition
- Stitching: 400 tiles \times 0.15 s/tile = 60 s ✓

Step 4: FCN Check for Battery Application

Adjust FCN weights for this application (resolution less critical, cost more critical):

$$C_{\text{score}}^{\text{batt}} = 0.2 \cdot \frac{\log_{10}(N_{\text{parallel}})}{9} + 0.5 \cdot \Gamma_{\text{mm}} + 0.3 \cdot (1 - \text{Cost}/\$1\text{M}) \quad (12.109)$$

For 2D system at \$500K:

$$C_{\text{score}}^{\text{batt}} = 0.2 \times 0.67 + 0.5 \times 0.85 + 0.3 \times 0.5 = 0.71 \quad (12.110)$$

Result: 2D planar architecture is the only viable option. Recommend simplified 2D system with:

- NA = 0.3 objective (off-the-shelf)
- 4-megapixel sCMOS (cost reduction)
- Automated XY stage for stitching
- Estimated system cost: \$450K

Worked Example 12.5: Multi-Physics FCN Enhancement

Problem: Evaluate how multi-physics capability changes the FCN ranking for 3D volumetric architecture.

Given: Single-physics FCN scores from Table 12.30 and Φ_{multi} factors: 0D = 1.0, 1D = 2.5, 2D = 3.0, 3D = 5.0.

Solution:

Step 1: Calculate Enhanced Capability Scores

Using Eq. (12.75):

$$C_{\text{score},0D}^{\text{multi}} = 0.47 \times (1 + \log_2(1.0)) = 0.47 \times 1 = 0.47 \quad (12.111)$$

$$C_{\text{score},1D}^{\text{multi}} = 0.68 \times (1 + \log_2(2.5)) = 0.68 \times 2.32 = 1.58 \rightarrow 1.0 \quad (12.112)$$

$$C_{\text{score},2D}^{\text{multi}} = 0.75 \times (1 + \log_2(3.0)) = 0.75 \times 2.58 = 1.94 \rightarrow 1.0 \quad (12.113)$$

$$C_{\text{score},3D}^{\text{multi}} = 0.72 \times (1 + \log_2(5.0)) = 0.72 \times 3.32 = 2.39 \rightarrow 1.0 \quad (12.114)$$

(Cap at 1.0 for normalized scoring)

Step 2: Recalculate FCN Composite

$$\text{FCN}_{0D}^{\text{multi}} = (0.87 \times 0.47 \times 0.26)^{1/3} = 0.48 \quad (\text{unchanged}) \quad (12.115)$$

$$\text{FCN}_{1D}^{\text{multi}} = (0.56 \times 1.0 \times 0.60)^{1/3} = 0.70 \quad (+15\%) \quad (12.116)$$

$$\text{FCN}_{2D}^{\text{multi}} = (0.65 \times 1.0 \times 0.53)^{1/3} = 0.70 \quad (+9\%) \quad (12.117)$$

$$\text{FCN}_{3D}^{\text{multi}} = (0.19 \times 1.0 \times 0.74)^{1/3} = 0.52 \quad (+16\%) \quad (12.118)$$

Step 3: New Rankings

Architecture	Single-Physics	Multi-Physics	Δ	New Rank
0D	0.48	0.48	0%	4
1D	0.61	0.70	+15%	1 (tie)
2D	0.64	0.70	+9%	1 (tie)
3D	0.45	0.52	+16%	3

Result: Multi-physics capability:

- Elevates 1D and 2D to “Strong candidate” threshold (0.70)
- Brings 3D into “Moderate candidate” range (0.52)
- Has no effect on 0D (no multi-physics advantage in single-NV systems)

Implication: For applications where multi-physics correlation is valuable (IC FA with correlated defects), 3D becomes more attractive despite low feasibility.

Worked Example 12.6: Complete System Design Using FCN

Problem: Design a production QFI system for semiconductor FA with the following requirements:

- Throughput: > 1000 sites/hour
- Resolution: < 1 μm
- Multi-physics: Magnetic + thermal
- Budget: \$800K

- Delivery: 18 months

Solution:

Step 1: FCN-Based Architecture Selection

From Table 12.30, 2D planar (FCN = 0.64) is the clear choice for production systems.

Step 2: Subsystem Specification from Error Budget

Target $\Gamma_{mm} \geq 0.85$ with balanced allocation:

Subsystem	Target Γ_i	Specification	Cost
Optics	0.96	Custom 0.8 NA snout, < 5% distortion	\$120K
MW System	0.94	Microstrip array, < 5% uniformity	\$80K
NV Diamond	0.97	3 ppm, 100 nm layer, < 10% variation	\$150K
Camera	0.98	sCMOS, 4 MP, 95% QE at 700 nm	\$60K
Control/DAQ	0.99	FPGA-based, real-time processing	\$90K
Software	0.98	GPU reconstruction, multi-physics fusion	\$100K
Integration	—	Assembly, calibration, validation	\$100K
Total	0.83		\$700K

Step 3: Risk Assessment

Primary risks from FCN analysis:

1. MW uniformity (highest technical risk)
2. Diamond supply (highest schedule risk)
3. Integration (highest cost risk)

Mitigation: Include \$100K contingency; qualify two diamond vendors; prototype MW antenna in Month 3.

Step 4: Throughput Verification

$$\text{FOV} = 200 \times 200 \mu\text{m}^2 \quad (12.119)$$

$$\text{Integration time} = 1 \text{ s (1 nT sensitivity)} \quad (12.120)$$

$$\text{Move time} = 0.5 \text{ s} \quad (12.121)$$

$$\text{Sites/hour} = \frac{3600}{1.5} = 2400 > 1000 \quad \checkmark \quad (12.122)$$

Result: Complete system specification with:

- FCN = 0.64 (Moderate-Strong candidate)
- $\Gamma_{mm} = 0.83$ (within 5% of target)
- Budget: \$800K (\$700K + \$100K contingency)
- Timeline: 18 months (achievable with parallel development)

12.11 Chapter Summary

This chapter established the system architecture framework for production QFI systems, with the following key contributions:

12.11.1 Key Results

1. **Architectural Taxonomy** (Section 12.3): Classification of 0D/1D/2D/3D architectures with quantitative trade-offs
2. **SWOT Analysis** (Section 12.4): Comprehensive evaluation showing 2D planar optimal for semiconductor FA (weighted score 3.7/5.0)
3. **Decoherence-Architecture Coupling** (Section 12.5): $T_2^{\text{eff}}/T_2^{\text{mat}} \approx 1/(1+\alpha C + \beta \log N)$
4. **Error Budget Framework** (Section 12.6): Multiplicative Γ_{mm} product with MW homogeneity as primary bottleneck
5. **FCN Framework** (Section 12.9): Novel quantitative methodology for technology assessment with geometric-mean composite score
6. **Multi-Physics Enhancement**: $C_{\text{score}}^{\text{multi}} = C_{\text{score}} \cdot (1 + \log_2(\Phi_{\text{multi}}))$

12.11.2 Design Rules Summary

Table 12.34: Chapter 12 Design Rules Summary.

Rule	Statement
DR 12.1	Architecture Selection: 2D planar for production FA; 0D for nm-scale research
DR 12.2	Error Budget Priority: Focus on lowest Γ_i ; target all $\Gamma_i > 0.95$
DR 12.3	FCN Threshold: FCN > 0.7 (strong), 0.5–0.7 (moderate), < 0.5 (weak)
DR 12.4	Investment Allocation: Proportional to $\text{FCN} \cdot \Delta\text{FCN}$
DR 12.5	MW Homogeneity: < 5% Rabi frequency variation for $\Gamma_{\text{mm}} > 0.90$
DR 12.6	Photonic Integration: Consider PIC for volumes > 100 units

12.11.3 Key Equations

Table 12.35: Key equations from Chapter 12.

Equation	Name	Reference
$\Gamma_{\text{mm}} = \prod_i \Gamma_i$	Model-Mismatch Product	Eq. (12.61)
$1/T_2^{\text{eff}} = 1/T_2^{\text{mat}} + \sum_i \gamma_i$	Effective Coherence	Eq. (12.55)
$\text{FCN} = (F_{\text{score}} \cdot C_{\text{score}} \cdot N_{\text{score}})^{1/3}$	FCN Composite	Eq. (12.74)
$C_{\text{score}}^{\text{multi}} = C_{\text{score}}(1 + \log_2 \Phi_{\text{multi}})$	Multi-Physics Enhancement	Eq. (12.75)

Problems and Solution Hints

Problem 12.1: FCN Score Calculation

A startup proposes a novel “2.5D” architecture using stacked waveguide layers with $N_{\text{parallel}} = 10^5$, TRL = 3, development cost = \$5M, achievable $\Gamma_{\text{mm}} = 0.80$, and two unique capabilities. Calculate the FCN composite score and determine if this is a viable investment.

Hint: Use Eqs. (12.69)–(12.74) with standard weights. The low TRL will significantly impact F_{score} .

Problem 12.2: Error Budget Optimization

A QFI system has $\Gamma_{\text{mm}} = 0.72$ with measured subsystem values: $\Gamma_{\text{opt}} = 0.92$, $\Gamma_{\text{MW}} = 0.88$, $\Gamma_{\text{NV}} = 0.94$, $\Gamma_{\text{cal}} = 0.96$, $\Gamma_{\text{drift}} = 0.97$. (a) Verify the product. (b) Identify the two primary bottlenecks. (c) Calculate the improvement needed in each to reach $\Gamma_{\text{mm}} = 0.85$.

Hint: (b) Compare to target of 0.95 for each Γ_i . (c) Assume other factors remain constant.

Problem 12.3: Architecture Selection

A biomedical application requires: 10 μm resolution, 1 cm^3 volume coverage, 10 minutes measurement time, room temperature operation. (a) Which architecture(s) could meet these requirements? (b) Calculate the FCN score for the viable option(s) with biomedical-specific weights.

Hint: (a) Throughput requirement determines architecture. (b) Adjust weights for biomedical: higher weight on Novelty (new market).

Problem 12.4: Multi-Physics Impact

Compare the FCN rankings for single-physics vs. multi-physics ($\Phi_{\text{multi}} = 4$) for all four architectures. At what Φ_{multi} value does 3D volumetric cross into the “Moderate candidate” threshold?

Hint: Use Eq. (12.75) and solve for Φ_{multi} such that $\text{FCN}_{3D}^{\text{multi}} = 0.50$.

Problem 12.5: Coherence-Architecture Trade-off

A 2D system has $T_2^{\text{mat}} = 1 \text{ ms}$ and architecture complexity $C = 4$. (a) Calculate T_2^{eff} using Eq. (12.56). (b) If dynamical decoupling extends coherence by factor of 5, what is the net T_2^{eff} ? (c) How does this impact C_{score} ?

Hint: (a) Use $\alpha = 0.05$, $\beta = 0.02$, $N = 10^6$. (b) Apply DD factor to T_2^{mat} .

Problem 12.6: Investment Portfolio

With a \$20M budget over 5 years, design an optimal investment portfolio across the four architectures using the FCN framework. Include: (a) Initial allocation (Year 1) (b) Re-evaluation criteria (when to shift investment) (c) Expected FCN evolution and go/no-go decision points

Hint: Use FCN evolution projections (Fig. 12.20); establish milestones based on TRL advancement.

References

- [1] L. Rondin et al., “Magnetometry with nitrogen-vacancy defects in diamond,” *Rep. Prog. Phys.* **77**, 056503 (2014).
- [2] J. F. Barry et al., “Sensitivity optimization for NV-diamond magnetometry,” *Rev. Mod. Phys.* **92**, 015004 (2020).
- [3] D. A. Broadway et al., “Quantum probe hyperpolarization of molecular nuclear spins,” *Nat. Commun.* **9**, 1246 (2018).
- [4] F. Dolde et al., “Electric-field sensing using single diamond spins,” *Nat. Phys.* **7**, 459–463 (2011).
- [5] V. M. Acosta et al., “Temperature dependence of the nitrogen-vacancy magnetic resonance in diamond,” *Phys. Rev. Lett.* **104**, 070801 (2010).
- [6] M. W. Doherty et al., “The nitrogen-vacancy colour centre in diamond,” *Phys. Rep.* **528**, 1–45 (2013).
- [7] P. Maletinsky et al., “A robust scanning diamond sensor for nanoscale imaging with single nitrogen-vacancy centres,” *Nat. Nanotechnol.* **7**, 320–324 (2012).
- [8] M. Pelliccione et al., “Scanned probe imaging of nanoscale magnetism at cryogenic temperatures,” *Nat. Nanotechnol.* **11**, 700–705 (2016).
- [9] D. Le Sage et al., “Optical magnetic imaging of living cells,” *Nature* **496**, 486–489 (2013).
- [10] E. V. Levine et al., “Principles and techniques of the quantum diamond microscope,” *Nanophotonics* **8**, 1945–1973 (2019).
- [11] I. Fescenko et al., “Diamond magnetic microscopy of malarial hemozoin nanocrystals,” *Phys. Rev. Appl.* **11**, 034029 (2019).
- [12] J. M. Taylor et al., “High-sensitivity diamond magnetometer with nanoscale resolution,” *Nat. Phys.* **4**, 810–816 (2008).
- [13] S. Bogdanov et al., “Material platforms for integrated quantum photonics,” *Opt. Mater. Express* **7**, 111–132 (2017).
- [14] N. H. Wan et al., “Large-scale integration of artificial atoms in hybrid photonic circuits,” *Nature* **583**, 226–231 (2020).
- [15] M. J. Burek et al., “High quality-factor optical nanocavities in bulk single-crystal diamond,” *Nat. Commun.* **5**, 5718 (2014).
- [16] A. Sipahigil et al., “An integrated diamond nanophotonics platform for quantum-optical networks,” *Science* **354**, 847–850 (2016).
- [17] C. Bradac et al., “Quantum nanophotonics with group IV defects in diamond,” *Nat. Commun.* **10**, 5625 (2019).
- [18] R. Schirhagl et al., “Nitrogen-vacancy centers in diamond: Nanoscale sensors for physics and biology,” *Annu. Rev. Phys. Chem.* **65**, 83–105 (2014).
- [19] K. Arai et al., “Fourier magnetic imaging with nanoscale resolution and compressed sensing speed-up using electronic spins in diamond,” *Nat. Nanotechnol.* **10**, 859–864 (2015).
- [20] G. Balasubramanian et al., “Nanoscale imaging magnetometry with diamond spins under ambient conditions,” *Nature* **455**, 648–651 (2008).